Bone 177 (2023) 116917

Contents lists available at ScienceDirect

Bone

journal homepage: www.elsevier.com/locate/bone

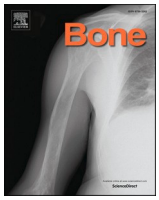

Full Length Article

Revolutionizing fracture fixation in diabetic and non-diabetic rats: High mobility group box 1-based coating for enhanced osseointegration

Alexandra Arteaga [a], Claudia Cristina Biguetti [b], BhuvanaLakkasetter Chandrashekar [a], Javier La Fontaine [b], Danieli C. Rodrigues [a,*]

[a] Department of Bioengineering, The University of Texas at Dallas, Richardson, TX, USA
[b] Department of Surgery and Biomechanics, School of Podiatric Medicine, The University of Texas Rio Grande Valley, Harlingen, TX, USA

ARTICLE INFO

Keywords:
Immunomodulation
Ionic liquids
Titanium
Osseointegration
Orthopedic implants
HMGB1
Rodent models

ABSTRACT

Chronic inflammation and hyperglycemia in diabetic patients increase the risk of implant failure and impaired fracture healing. We previously developed and characterized a titanium (Ti) coating strategy using an imidazolium-based ionic liquid (IonL) with a fully reduced, non-oxidizable High Mobility Group Box 1 (HMGB1) isoform (Ti-IonL-HMGB1) to immunomodulate tissue healing. In this study, we used an open reduction fracture fixation (ORIF) model in non-diabetic (ND) and diabetic (D) rats to further investigate the effectiveness of this Ti-IonL-HMGB1 coating on orthopedic applications. Ninety male Lewis rats (12–15 weeks) were divided into D (n = 45) and ND (n = 45) groups that were distributed into three subgroups based on the type of local treatment received: Ti (uncoated Ti), Ti-IonL, and Ti-IonL-HMGB1 implants. Fracture healing and osseointegration were evaluated using microtomographic, histological, and immunohistochemical analysis of proliferating cell nuclear antigen (PCNA), Runt-related transcription factor 2 (RUNX2), and HMGB1 markers at 2, 10, and 21 days post-ORIF. Scanning Electron Microscopy verified the coating stability after placement. Microtomographic and histological analysis demonstrated increased fracture healing and osseointegration for ND rats in all treatment groups at 10 days, with impaired healing for D rats. Immunohistochemical analysis exhibited elevated PCNA+ and RUNX2+ cells for D animals treated with Ti-IonL-HMGB1 at 21 days compared to all other groups. The immunohistochemical marker HMGB1 was elevated at all time points for D animals in comparison to ND animals, yet was lowered for D tissues near the Ti-IonL-HMGB1 treated implant. Improved osseous healing was demonstrated in D animals with Ti-IonL-HMGB1 treatment by 21 days, compared to D animals with other treatments. To the best of our knowledge, this is the first study analyzing Ti-IonL-HMGB1 implantation in an injury site through ORIF procedures in ND and D rats. This surface approach has potential for improving implanted biomaterials in diabetic environments.

1. Introduction

Although Titanium (Ti) orthopedic devices have been shown to be effective in restoring the function of fractured bones, diabetic patients often experience higher risk for osseointegration failure and fracture union compared to non-diabetic patients [1–6]. Approximately 9 % of all lower extremity fractures occur in ankles [7–9], and an estimated one out of every eight patients undergoing ankle fracture fixation surgeries are diabetic [10,11]. The diabetic population has historically had poor clinical outcomes/complications from Ti implantation ranging from 26 to 47 % compared to 15 % in the non-diabetic population [9,10,12]. Compromised osseointegration in diabetics can occur due to infection, corrosion, or ion leaching of the implant surface that can all lead to chronically upregulated inflammatory responses that result in reduced bone healing and impaired fracture fixation [13–16]. Even in the absence of these events, diabetes by itself leads to delayed inflammatory resolution post injury and delayed tissue healing, which ultimately favors the occurrence of the other above cited factors [13–16]. Patients with Type 1 diabetes normally have a lower bone mineral density (BMD) and increased fracture risk, primarily due to insulin deficiency and metabolic imbalances [17,18]. Type 2 diabetic patients have more variability on their BMD, which is often influenced by factors like body composition and medication use [17,18]. Additionally, poorly controlled blood glucose levels can impair various aspects of the bone

* Corresponding author at: Department of Bioengineering, University of Texas at Dallas, 800 West Campbell Road, Richardson, TX, USA.
E-mail address: danieli@utdallas.edu (D.C. Rodrigues).

https://doi.org/10.1016/j.bone.2023.116917
Received 11 July 2023; Received in revised form 16 September 2023; Accepted 18 September 2023
Available online 20 September 2023

healing process, such as collagen formation, osteoblast function, and immune response, leading to delayed healing and increased complications [19,20]. Thus, optimizing the inflammatory microenvironment for a favorable healing response is crucial for the successful integration of implant systems in challenging biological conditions.

Upon Ti implantation, surgical trauma results in the release of High Mobility Group Box 1 (HMGB1) that is shown to trigger immune response and tissue healing [21,22]. HMGB1 is a redox sensitive molecule that has been proven to be fundamental in inflammation, Ti osseointegration, and bone healing post-trauma [22,23]. HMGB1 can exist in three different isoforms that each have different biological functions: "fully-reduced HMGB1" (FR-HMGB1), "disulfide HMGB1" (DS-HMGB1) and inactive "sulfonyl HMGB1" [23,24]. FR-HMGB1 is passively released from necrotic cells and is involved in the recruitment of stem cells into healing tissues [23]. However, FR-HMGB1 can be oxidized by increased amounts of reactive oxygen species (ROS) in pro-inflammatory environments and be converted into DS-HMGB1 or be inactivated into a sulfonyl isoform. Immunocompromised conditions, such as in an uncontrolled diabetic environment, are linked to increased reactive oxygen species (ROS) [25]. Thus, in a diabetic environment, FR-HMGB1 could be rapidly converted to DS-HMGB1 resulting in the induction of pro-inflammatory pathways, which can negatively impact healing outcomes [24,26]. Nevertheless, a recombinant fully-reduced and non-oxidizable isoform of the HMGB1 was recently developed to where three cysteines were replaced by serines(3-Serine HMGB1 (3S-HMGB1)), which was demonstrated to prevent the oxidation pathway from ROS [27].

Considering HMGB1 as a potential therapeutic protein, a previous study demonstrated that the inhibition of the released isoform (FR-HMGB1 from necrotic cells) of this protein using Glycyrrhizic Acid led to impaired osseointegration in a mouse model [22]. Another study then showed that the direct local administration of FR-HMGB1 and the 3S-HMGB1 to the fracture sites of a mouse model led to accelerated osteogenic differentiation, while the administration of the proinflammatory DS-HMGB1 did not induce an osteogenic response [23]. However, this last study did not investigate osseointegration associated with hardware implantation, but aimed at the administration of HMGB1 solely in the fracture gap in non-diabetic animals.

In order to understand the interactions between HMGB1 and a Ti surface, we previously demonstrated that HMGB1 can have direct and irreversible adsorption onto Ti surfaces. The study showed that such adsorption can denature HMGB1 at implantation sites, impacting its beneficial biological functions [28]. These previous observations indicate that the direct delivery of HMGB1 to implantation sites could be targeted and optimized by utilizing a non-interfering coating that preserves its biological binding sites and enables gradual release post-implantation [28]. Prior studies of dicationic imidazolium-based ionic liquids (IonL) have demonstrated antimicrobial, anti-corrosive, lubricative and biocompatible properties [29–32]. Considering the multifunctional benefits of IonLs, they were employed as a coating strategy to both attach and prevent the direct adherence of exogenous HMGB1 onto Ti surfaces. It forms a thin film on Ti surfaces, shielding the protein and preventing direct attachment to the Ti surface, while still strongly interacting with HMGB1 [33]. Our previous results pointed out that the miscibility of the IonL with water caused a gradual release of HMGB1 after implantation [33]. Finally, we demonstrated that both FR-HMGB1 and 3S-HMGB1 on Ti-discs are biocompatible and promote tissue healing, while DS-HMGB1 chronic inflammation [34] and delayed tissue healing after subcutaneous implantation in Lewis rats. Of note, in this previous study we tested for the biocompatibility of different HMGB1 isoforms using IonL as an anchoring molecule. These coatings were all tested in adult male non-diabetic Lewis rats.

Open reduction internal fixation (ORIF) using metallic implants are the standard procedure for ankle fractures treatment in diabetic patients. Thus, in the present study, we used a clinically relevant ORIF model to evaluate fracture fixation [35] to investigate the efficacy of 3S-HMGB1 (which will be referred to as "Ti-IonL-HMGB1") on osseous fracture healing and osseointegration in non-diabetic (ND) and diabetic (D) Lewis rats. Up to date, there has been no investigation of the impact of 3S-HMGB1 associated to a coating to accelerate osseointegration in D conditions. We first employed scanning electron microscopy (SEM) to evaluate coating stability after screw insertion into the bones. Following the ORIF procedure in ND and D rats, the impact of the coating on osseointegration and fracture healing was assessed using MicroCT, histological and molecular characterization.

Considering the increasing number of diabetic patients that require orthopedic interventions, it becomes crucial to design implants that will gear the inflammatory response toward predictably positive healing outcomes. Successful osseointegration outcomes of ORIF procedures can be hampered by surrounding inflammatory conditions that arise from chronic hyperglycemic environments, infections, or implant-associated corrosion [20]. Diabetic patients often have higher risk of complications with ankle fractures due to chronic inflammatory responses that lead to reduced wound healing capabilities[126]. Thus, the aim of this study was to use a clinically relevant, and reproducible surgical procedure, ORIF model, to assess how the innovative Ti-IonL-HMGB1 coating affects normoglycemic and diabetic tissues.

Current approaches to engineer Ti surfaces include physical (modifications in surface topography and wettability) and chemical (ceramic coating, synthetic or peptide immobilization) to modulate tissue responses [36,37]. However, the continuation of complications from non-diseased scenarios have been a significant incentive to improve implanted biomaterials [38]. Successful osseointegration occurs when a protein layer gets adsorbed onto the implant surface and recruits and induces the migration, proliferation and differentiation of key cells related to bone healing [22,39,40]. Our group has used a well characterized, multifunctional IonL [29–32,41–45] as a thin film to immobilize key immunomodulatory proteins, such as HMGB1, to functionalize an implant surface and harness the immune response. It was previously demonstrated in vitro and in silico that the IonL used in this study could pre-immobilize HMGB1 in a biologically active conformation [33]. Our group has also proposed that a commercially available, non-oxidizable isoform of HMGB1 be used for further orthopedic studies (Ti-IonL-HMGB1), based on our prior in vivo results using a subcutaneous model in Lewis rats [34]. However, the performance of this Ti-IonL-HMGB1 was still unknown in normoglycemic or diabetic conditions.

2. Materials and methods

2.1. Coating preparation

1,10-Bis(3-methylimidazolium-1-yl)decane diphenylalanine (IonL) was synthesized following the Fukumoto et al [46] and Shirota et al [47] methods, where the amino acid and dicationic structure were created, respectively. The IonL was then characterized using previously established protocols [29,30,32,48]. IonL-Phe was characterized using 1H nuclear magnetic resonance spectroscopy (NMR) (Bruker Avance III-HD 600 NMR, Bruker, Billerica, MA, USA), and the data found was in accordance with the literature [29,30,48]. 3S-HMBG1 (REHM130 HMGB1) was purchased from Tecan IBL International.

2.2. Sample preparation

Grade 2 commercially pure titanium (cpTi) pins (0.76 mm ⌀ × 2 mm Stabilok™, Fairfax Dental Inc., Miami, FL, USA) were used as orthopedic implants in this study. All implants were cleaned by ultrasonication for 15 min intervals in acetone, DI water, and ethanol solutions, respectively. After sonication, implants were dried in an oven at 65 °C overnight and sterilized in an autoclave.

Experimental samples receiving the IonL coating (Ti-IonL and Ti-IonL-HMGB1) were first dip coated in 50 mM ethanolic solution of IonL for 10 min. Samples were then removed from the solution at a

constant rate of 60 μm/s with the assistance of a motorized stage (TA Instruments, New Castle, DE, USA) to create a uniform coating, and then dried in an oven at 65 °C for 48 h to achieve a final dose of 0.1 μmol IonL on each disk after drying, according to previous literature [32]. Characterizations of IonL-based coatings on Ti have been performed in previous studies through cytotoxic, antimicrobial, cytocompatibility, tribological and anti-corrosive evaluations [29–31,41–44]. A previous study in mice found that relevant biological doses of exogenous HMGB1 vary from 2.25 μg to 22.5 μg injected directly to the injury site, with optimal effect dose of 22.5 μg per mouse (0.75 mg/kg) [23]. Thus, after drying in an oven at 65 °C for 48 h, samples receiving HMGB1 (HMGBiotech, Milano, Italy) were subsequently drop-coated with 2.5 μg of 3S-HMGB1 (Ti-IonL-HMGB1) diluted in 2.5 μL of deionized water and dried for 1 h at room temperature, which represents a final dose of 0.75 mg/kg of HMGB1 per rodent among both screws. All procedures were performed in a biosafety cabinet using aseptic techniques to ensure sterile conditions.

2.3. Animals and experimental design

A total of 90 Lewis rats, male,12–15-weeks old were purchased from Charles River at 3 weeks of age and were housed in the vivarium throughout the study. Sterile water and dry food pellets were available to rats ad libitum. All anesthetic, surgical, and post-operational procedures as well as diabetes induction were approved by the institutional animal care and use committee (IACUC) #19–03. First, animals equally divided in two groups of 45 rats of diabetic (D) and non-diabetic (ND). At 6 weeks of age, food for the D group was changed to a high fat diet (Purina 5008) for a minimum of 6 weeks (see Diabetes Induction below) and remained available ad libitum. Five (5) animals per systemic condition/treatment group/time point were euthanized at 2, 10, and 21 days post ORIF procedure for collection of tibias.

2.4. Diabetes induction

For diabetes induction of the D group, 6-week-old rats were fed a high fat diet (Purina 5008) for a minimum of 6 weeks, followed by a single dose of streptozotocin (STZ) (intraperitoneal injection of 55 mg/kg) using previously established protocols [35]. ND rats were fed the standard diet and treated equal volumes of saline solution, based on their body weight. Glucose levels were analyzed at 3 days post-STZ administration for the D group and compared to the ND animals to confirm D induction. In addition, glucose levels were taken before surgeries and before euthanasia at the end of each time point. Fasting blood glucose levels were evaluated after 6 h of fasting for both D and ND animals. Approximately 30uL of blood was collected from the tail vein and evaluated using a glucometer (AlphaTRAK 2 Blood Glucose Monitoring System Kit). Rats were temporarily anesthetized using 4 % isoflurane inhalation to avoid stress during the blood sample collection. Water consumption was also measured by weight 5 days pre- and post-STZ injection. For the insulin resistance test, Insulin (Humulin R U-100, (0.75 IU/kg) was administered by intraperitoneal injection after 6 h of fasting. Fasted blood glucose measurements were performed with a glucometer at 0-, 30-, 60-, and 120-min post insulin injection. After euthanasia, pancreas samples from ND and D rats were collected to be evaluated through histopathological analysis.

Previous studies revealed that mortality occurred within a week of STZ injection (50–65 mg/kg) and was significantly increased with animal age (3 % at 6–11 weeks, 83 % at 12–17 weeks, and 91 % at >18 weeks) [49]. High-dose STZ severely impaired insulin secretion, which mimicked type 1 diabetes [50]. Low-dose STZ induced a mild impairment of insulin secretion, similar to later stages of type 2 diabetes [51]. Previous studies that have used HFD and STZ also had varied time frames for the HFD (ranging from 2 to 10 weeks), number of STZ doses (1–2 doses), or amounts of STZ given (30–45 mg/kg per dose) [51–54].

2.5. ORIF surgical procedure

ORIF procedure followed previously established protocols using Lewis rats [35]. Body weights of each rat was monitored before and after surgery. Systemic conditions were verified prior to surgery by blood glucose measurements. Lewis rats were first anesthetized by inhalation of 4 % isofluorane followed by injection of ketamine:xylazine (50–100 mg/kg: 20 mg/kg IP). Following anesthesia, rats were placed in a left lateral decubitis position on a surgical table. For the ORIF procedure, a vertical incision was created directly below the right knee joint, followed by tibial tuberosity exposure by muscle divulsion using a periosteal elevator. A vertical osteotomy (0.1 mm in width, 4 mm in length and 3 mm in depth) was created on the tibia with a circular saw (1,800,020 Fine Science Tools, Foster City, CA, USA) using a surgical micromotor at 800 RPM (NSK Surgic Pro) under constant irrigation with cold saline solution to avoid heating. Commercially pure titanium (cpTi) threaded dentin screws (0.76 mm ⌀ x 3.5 mm, Fairfax Dental Inc., Miami, FL, USA) were then used for osteotomy fixation. Two pins (Ti (uncoated Ti), Ti-IonL, or Ti-IonL-HMGB1) were placed using microneedle holders in a perpendicular position in relation to the osteotomy at a distance of 2 mm between pins, which was determined using an angled 3.25" Dental Castroviejo Caliper. Surgical protocol followed a previously established procedure [35]. During surgery, animals will receive Lidocane HCl/Epinephrine (1:100,000). After surgery, all animals received Buprenorphine (0.3 mg/kg, SC) as analgesia every 12 h for 72 h, and Cefazoline (5 mg/kg, intramuscular) as an antibiotic. Animals were humanely euthanized at 2, 10 and 21 days by inhalation of 4 % isofluorane, followed by injection of ketamin/xylazine (50 mg/kg: 20 mg/kg intraperitoneal), and subsequently with sodium pentobarbital (120 mg/kg, intraperitoneal) overdose. Animals were euthanized at different times points (2, 10 and 21 days) with previously mentioned anesthesia followed by an overdose of pentobarbital sodium (Euthanasia III Med-Pharmex Inc., Pomona, CA, USA). Tibias were collected immediately after euthanasia and submerged in 10 % neutral buffered formalin for 24 h for fixation. Samples were continuously washed in water for 24 h after fixation to prevent over fixing and subsequently placed in 70 % ethanol until microCT imaging. Control tibias (with no surgery) were removed upon sacrifice and used for further studies to characterize coating stability pre- and post-implantation of implants (Ti (uncoated Ti), Ti-IonL, or Ti-IonL-HMGB1).

2.6. Scanning Electron Microscopy for coating stability

Three tibias from control right legs of ND animals were obtained upon euthanasia. Soft tissues and bone marrow were removed, rinsed with saline and air dried. Extracted tibias underwent ORIF procedure. Treatment implants (Ti, Ti-IonL, and Ti-IonL-HMGB1) were prepared, as previously noted, and analyzed before and after insertion by Scanning Electron Microscopy (SEM) (JEOL, JSM6360LV, Akishima, Japan) to verify the presence of the coating. To avoid reverse torque and damaging of coating during implant retrieval, bones were cut using a circular bone saw and implants were carefully retrieved without touching the threads and compromising the coating.

2.7. Microtomographic analysis

Controls and treated tibias were imaged using ultra-high-resolution micro-CT imaging (OI/CT, Milabs, Utrecht, Netherlands) at a voltage of 50 kV, a current of 0.21 mA, and an exposure time of 75 ms for evaluation of fracture healing by means of bone volume fraction measurements (BV/TV %). Projections were then reconstructed at a voxel size of 20 μm using vendor software and converted to DICOM (Digital Imaging and Communications in Medicine) files using PMOD analysis software (PMOD Technologies LLC, Zurich, Switzerland). Quantification of bone parameters were performed using Imalytics Preclinical (Gremse-IT GmbH, Aachen, Germany). Meta diaphyseal region of tibia of

specimens was analyzed using a spherical region of interest (ROI) 3 mm in diameter, positioned in the cortical area. Cortical analysis included the acquisition of bone volume (BV, mm^3), tissue volume (TV, mm^3), and bone volume fraction (BV/TV %). BV and TV in cortical bone in the mid-diaphysis were analyzed using cylindrical ROIs 1 mm ⌀ by 1 mm in length. Tibias from D and ND animals that did not undergo ORIF procedure were evaluated as controls.

2.8. Histological samples

After microCT imaging, tibial samples were subjected to a decalcification protocol using 10 % ethylenediaminetetraacetic acid (EDTA)-2Na (Sigma, St. Louis, MO, USA), with two fresh EDTA changes per week. Tibias were reduced to $10mm^2$ sections of tissue surrounding the implant areas, which were then processed for paraffin embedding using a tissue processor (Leica ASP300 S) for 12 h. Implants were carefully removed from tibias (using microneedle holders [45]) and mounted in paraffin blocks. Sets of 5 μm histological sections (technical replicates) were obtained from each biological replicate at the titanium implantation site. Sectioned tibial samples were stained with hematoxylin and eosin (H&E) for analysis of the cellular content and Goldner Trichrome (GT) with Alcian Blue [55] for evaluation of the bone and cartilaginous matrix surrounding the implants, as well as for analysis of bone to implant contact. Quantification of H&E and GT analysis was conducted by three reviewers using ImageJ software (Version 1.51, National Institutes of Health, Bethesda, MD, USA).

2.9. Bone to implant contact analysis

Osseointegration was assessed for bone to implant contact (BIC%) using GT staining in tibial tissues surrounding each implant treatment. Three technical replicates were evaluated using 6 histological fields per replicate. The best representative section of each treatment group at the 21-day time point was stained with GT and used to measure BIC% as previously described [45,56]. Images for BIC% were analyzed and quantified using Cellsens software (Olympus, Shinjuku City, Tokyo, Japan); BIC% was determined by calculating the percentage of cortical bone in direct contact with the implant (defined by the implant space) relative to the entire implant length at the cortical bone level. Data from BIC% were analyzed for statistical significance ($n = 6$, $p < 0.05$) and results were presented as mean +/− standard deviation (SDs).

2.10. Immunohistochemistry

Immunohistochemistry was used to identify and quantify positive cells for the following markers: PCNA (Proliferating cell nuclear antigen), RUNX2 (Runt-related transcription factor 2), and HMGB1 (High Mobility Group Box 1). Dark brown staining indicated cells expressing PCNA, RUNX2, or HMGB1, which were quantified as positive cells. Markers were assessed in the fracture gap area and in surrounding the Ti threads. Histological sections at the titanium implantation sites from each biological replicate were deparaffinized and submerged for antigen retrieval in Citrate Buffer (pH 6.0) at 95 °C for 30 min. Tibial tissues were washed with 1× phosphate buffered saline (PBS) (pH 7.4) and deionized (DI) water, followed by a blocking step with 1 % bovine serum albumin (BSA) (10 mg/mL, in 1× PBS, Sigma-Aldrich, St. Louis, MO, USA) and incubated with the selected primary antibody. Primary antibodies were purchased from Abcam and diluted in the following concentrations: PCNA (ab92552) at 1:1000, RUNX2 at 1:500 (ab236639), and 1:400 HMGB1 (ab79823). All samples were individually tested with each primary antibody; following primary antibody application, samples were incubated overnight in a humidified chamber at 4 °C. The following day, primary antibodies were subsequently incubated with rabbit specific Horseradish Peroxidase (HRP)/ 3, 3′-diaminobenzidine (DAB) (Avidin–Biotin Complex (ABC)) and Micropolymer Detection IHC Kit (Abcam, Cambridge, UK). Three independent measurements from each animal were stained with each marker for analysis. A negative control was additionally incubated with BSA (10 mg/mL, in 1× PBS) instead of a primary antibody to confirm specific binding of the secondary antibody. Slides were then washed with 1× PBS and incubated for 10 min with hydrogen peroxide solution. Slides were washed in 1× PBS 3 times and incubated with Micropolymer Abcam IHC kit, followed by a 1 min incubation with 3,3′-diaminobenzidine (DAB) chromagen. As a final step, all samples were counterstained in Mayer's Hematoxylin for 2 min, and mounted with Permount (Fisher Scientific, Hampton, NH, USA) and a coverslip. Using ImageJ software, positively (+) stained cells for each marker were quantified by creating a grid image with 108 points superimposed on each histological field; the total number of points were obtained to calculate the area density (%) for each marker.

2.11. Statistical analysis

Statistical tests for MicroCT data, BIC%, and immunohistochemistry were selected according to the distribution of normality of datasets by the Shapiro-Wilk Normality test. As all groups passed the normality test, statistical analyses were performed using a two-way analysis of variance (ANOVA) with a post hoc Tukey test considering time and treatments (Ti, Ti-IonL, or Ti-IonL-HMGB1) as factors. The Tukey test made multiple comparisons to evaluate the significance between the factors. Analysis was run in GraphPad Prism 5.0 software (GraphPad Software Inc., San Diego, CA, USA) using a significance level (α) of 0.05. Statistical significance of comparisons between different data sets ($n = 6$ independent measurements) was determined using the p value.

3. Results

3.1. Implant coating stability post open reduction internal fixation procedure

SEM analysis was used to visualize coating morphology on the screws pre- and post-implantation. Uncoated Ti screws demonstrated rough surface morphology pre-implantation, while presenting adherent biological debris pos-implantation. Prior to implantation, the IonL was gathered in the ridges of the screws (demonstrated by the green arrows) for Ti-IonL screws. Ti-IonL screws also demonstrated fewer biological debris compared to the uncoated Ti post-implantation. Ti-IonL-HMGB1 coated screws resulted in crystal-like formation (demonstrated by red arrows) that remained present post-implantation (Fig. 1).

3.2. Validation of diabetes induction throughout the study

We performed several tests to validate D induction and to ensure all D rats and local treatment subgroups were under chronic hyperglycemia during the study. Before the ORIF procedures, ND and D rats were evaluated for water consumption 5 days pre- and 5 days post-STZ injection. Overall, ND rats consumed an average of 61.90 ± 7.79 g of water daily. After 5 days, the water consumption was significantly higher for D rats compared to ND rats ($p < 0.001$). D rats consumed 57.44 ± 8.17 g prior to injection and consumed a final weight of 269.60 ± 21.48 g of water per cage daily (Fig. 2A).

For insulin resistance testing, ND rats initially started with an average fasted blood glucose of 96.75 ± 9.53 mg/dL, which dropped to 69.25 ± 5.56 mg/dL at 15 min after insulin administration. Control rats then maintained an average fasted blood glucose of 69.13 ± 7.60 mg/dL from 30 to 120 min after insulin administration. HFD + STZ rats, commenced the insulin resistance test with an average fasted blood glucose of 606.00 ± 133.11 mg/dL, that dropped to the lowest level of 353.50 ± 47.15 mg/dL at 30 min, and rebounded to a final level of 480.25 ± 141.11 mg/dL at the 120 min post-insulin injection. ND rats that were fed a HFD maintained an average fasted blood glucose of 94.75 ± 17.23 mg/dL from the initial time point through 90 min after insulin injection, then increased to 141.00 ± 41.58 mg/dL, with no

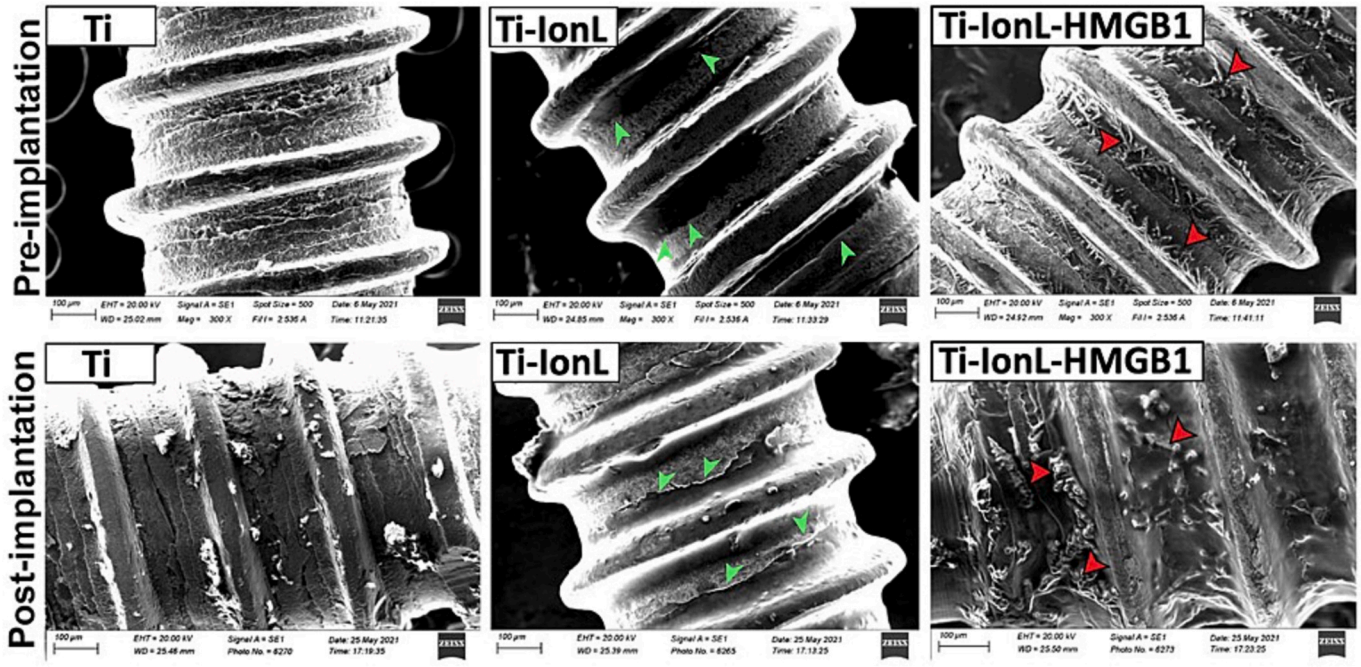

Fig. 1. SEM images illustrating uncoated (Ti), ionic liquid (Ti-IonL) and HMGB1 (Ti-IonL-HMGB1) screws pre- and post-implantation taken at 300× magnification. Green arrows demonstrated IonL, while red arrows demonstrate the HMGB1 crystal-like formations. (For interpretation of the references to colour in this figure legend, the reader is referred to the web version of this article.)

significant difference compared to the control group (Fig. 2B).

Histological samples from ND and D pancreas ($n = 3$ independent qualitative analyses per systemic condition) were stained by H&E and analyzed for histopathological changes in islets containing insulin-secreting beta-cells. While normal and large pancreatic islets were observed in ND rats, important atrophy and vacuolation were found in pancreatic islets of all D rats (Fig. 2C). MicroCT analysis of 3 independent control tibia ($n = 3$), analyzed at 6 different regions within each tibia, qualitatively demonstrated reduced cortical region areas in D animals compared to ND animals (Fig. 2D).

3.3. Clinical outcomes after open reduction internal fixation procedure

All animals showed normal signs of mobility and had a 100 % survival rate from the surgery. Acute pain produced post-surgically was evaluated as minimal based on facial actions, orbital tightening, nose/cheek flattening, ear changes and whiskers were in accordance with the Rat Grimace Scale [57].

Average fasted blood glucose levels were evaluated for both ND and D animals immediately before ORIF procedures and prior to euthanasia. Data is demonstrated for 21 days, since this is the longer time point. Mean (SD) for blood glucose levels for ND rats were consistently <250 mg/dL before (Ti: 110.20 ± 14.24 mg/dL, Ti-IonL: 121.20 ± 14.55 mg/dL, and Ti-IonL-HMGB1: 164.80 ± 35.51 mg/dL) and 21 days after surgery (Ti: 172.20 ± 21.32 mg/dL, Ti-IonL: 159.60 ± 30.45 mg/dL, and Ti-IonL-HMGB1: 218.60 ± 24.66 mg/dL). Alternatively, mean glucose values for D rats were consistently >250 mg/dL, confirming the D status for this animal model, and significantly higher than the ND counterpart before (Ti: 407.60 ± 16.13 mg/dL, Ti-IonL: 469.60 ± 36.73 mg/dL, and Ti-IonL-HMGB1: 544.60 ± 27.40 mg/dL; $p \leq 0.0001$) and 21 days after surgery (Ti: 403.20 ± 60.46 mg/dL, Ti-IonL: 370.00 ± 41.28 mg/dL, and Ti-IonL-HMGB1: 382.40 ± 22.35 mg/dL; $p \leq 0.0001$) for all treatment groups(Fig. 3A and Table S1). Additionally, Ti-IonL-HMGB1 D animals were significantly higher than Ti-IonL D ($p \leq 0.001$) and uncoated Ti D ($p \leq 0.001$). These results indicated that higher glucose levels were maintained in D animals during the treatments compared to ND animals.

Both ND and D animals were weighed prior to each surgical procedure and euthanasia. Average weights remained consistent regardless of systemic condition or treatment. However, a significant difference was noted between ND and D animals treated with Ti-IonL-HMGB1 D the 21-day post-surgical time point (ND: 416.80 ± 15.11 g and D: 366.60 ± 15.27 g; $p < 0.05$). Results for animal weights are shown in Fig. 3B and Table S2.

3.4. Microtomographic analysis and histological outcomes post open reduction internal fixation procedure

The microCT analysis revealed the bone quality of both the site of Ti implantation and the fracture site of ND and D groups at each time point in response to each treatment ($n = 6$ independent, qualitative analyses per systemic condition, time point, and treatment). As observed in Fig. 4, the fracture defect (demonstrated by green arrows) was present for all treatment groups and systemic conditions at 2- and 10-day time points. At 21 days, the fracture was not seen in any treatment groups for the ND group (0/27 ND animals at the 21-day time point) yet remained present in the D group for Ti and Ti-IonL samples (18/27 D animals at the 21-day time point). Of particular significance, the D group treated with Ti-IonL-HMGB1 (9/27 D animals) demonstrated signs of fracture closure at 21 days post-implantation that was comparable to the ND group.

Histological evaluation using H&E and GT with Alcian Blue-stained samples further demonstrated fracture healing (Fig. 5) and osseointegration (Fig. 6) of ND and D groups in response to treatment groups over 2, 10 and 21 days. At the 2-day time point, it was possible to identify proper blood clot formation at the fracture and screw areas in ND and D rats for all treatment groups (Ti, Ti-IonL and Ti-IonL-HMGB1). At 2 days, blood clots were present in all groups at the fracture and screw areas, which corresponded to hematoma formation and inflammatory events. At the 10-day time point, ND rats treated only with uncoated Ti (which represents a negative control), presented initial new bone formation through new trabeculae permeating the fracture area and surrounding the screw thread spaces (Fig. 5). Similar results and pattern of fracture healing were observed in ND rats treated with Ti-IonL and Ti-IonL-HMGB1 implants. Of note, all these groups presented the new bone

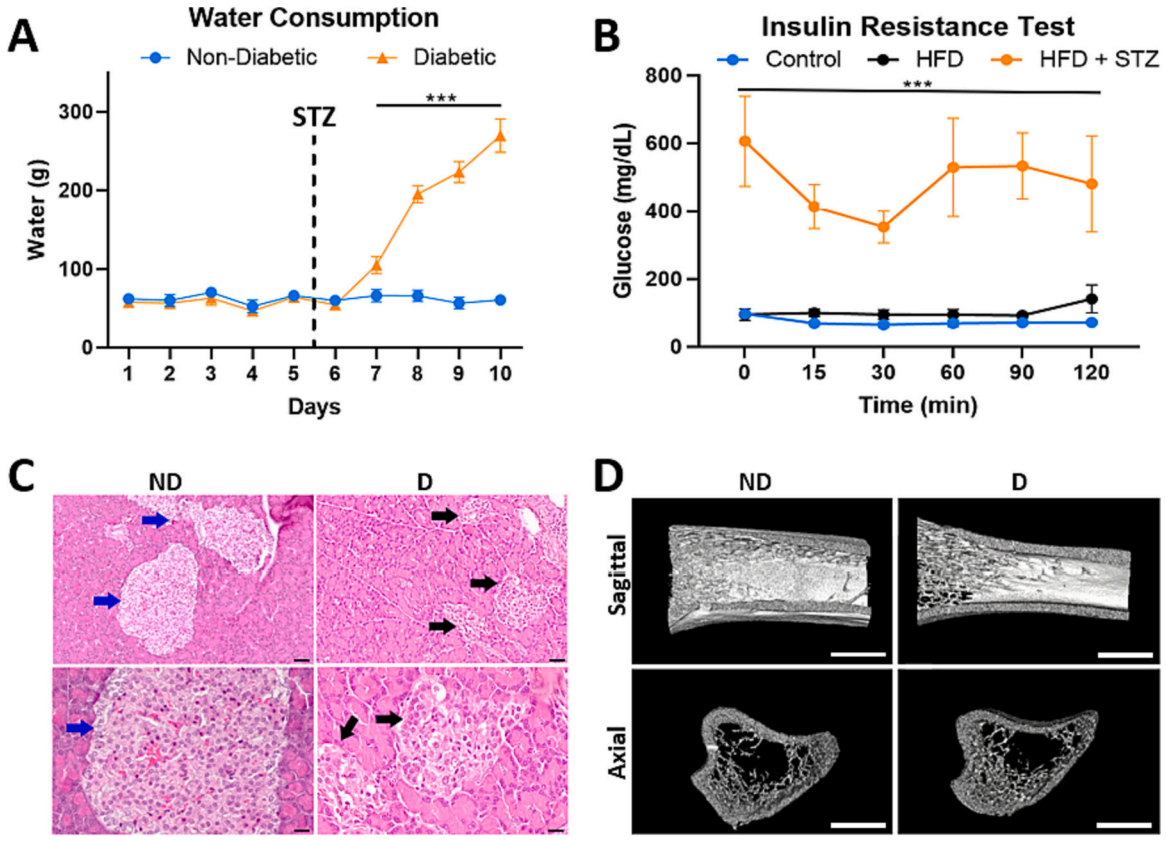

Fig. 2. Clinical evaluation of ND and D rats through water consumption (g) before and after STZ-diabetes induction (n = 3 cages and 2 rats per cage) *(A)*. Mean concentration of glucose (mg/dL) was taken over time during an insulin resistance test post IP glucose injection for control, high fat diet (HFD) and diabetic (HFD + STZ) rats ($n = 5$) *(B)*. Histological evaluation of pancreatic samples in ND and D rats (n = 3 per systemic condition). Scale bar = 100 μm (top), 20 μm (bottom), staining: H&E, original magnification 40× *(C)*. The blue arrows show normal pancreatic islet containing insulin-secreting beta-cells and blood vessels in ND rats. The black arrow shows atrophic pancreatic islet in D rats. Sagittal and axial microCT images of control tibia for ND and D Lewis rats at 21 days *(D)*. Scale bar = 3.5 mm. Symbol *** indicates statistical significance as compared to ND control groups ($p \leq 0.001$). (For interpretation of the references to colour in this figure legend, the reader is referred to the web version of this article.)

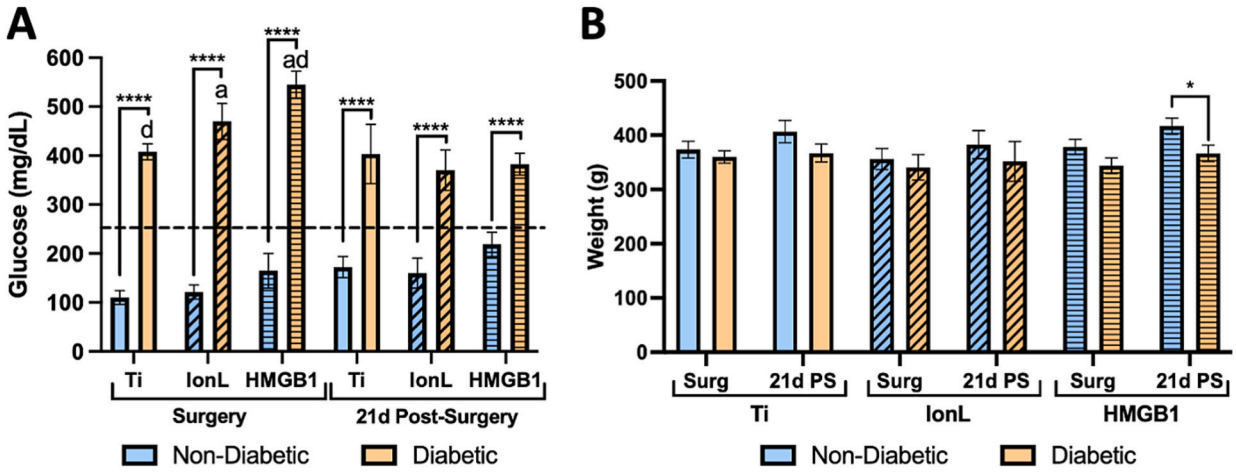

Fig. 3. Graphical quantification of blood serum glucose levels *(A)* and animal weights *(B)* in non-diabetic and diabetic rats. Data is shown as means ± SD for glucose (mg/dL) and weights (g) with significance between systemic condition (non-diabetic vs. diabetic; * = $p \leq 0.05$, ** = $p \leq 0.01$, *** = $p \leq 0.001$) and between treatments ((Ti), ionic liquid coated (IonL = Ti-IonL) and IonL-HMGB1 coated Ti (HMGB1 = Ti-IonL-HMGB1; a: $p \leq 0.05$ and d: $p \leq 0.0001$) at the time of surgery and 21 days post-surgery (21d PD) ($n = 5$). Black dotted line represents the systemic condition threshold (250 mg/dL) for ND (< 250 mg/dL) and D (>250 mg/dL) groups.

surrounded by a loose connective tissue that was rich in new blood vessels, which were converted into a mature bone marrow space at 21-day time point.

Conversely, the D group treated with uncoated screws (D—Ti) presented minimal new bone formation at the bone edges surrounding the fracture. A predominance of dense connective tissue, rich in fibers and

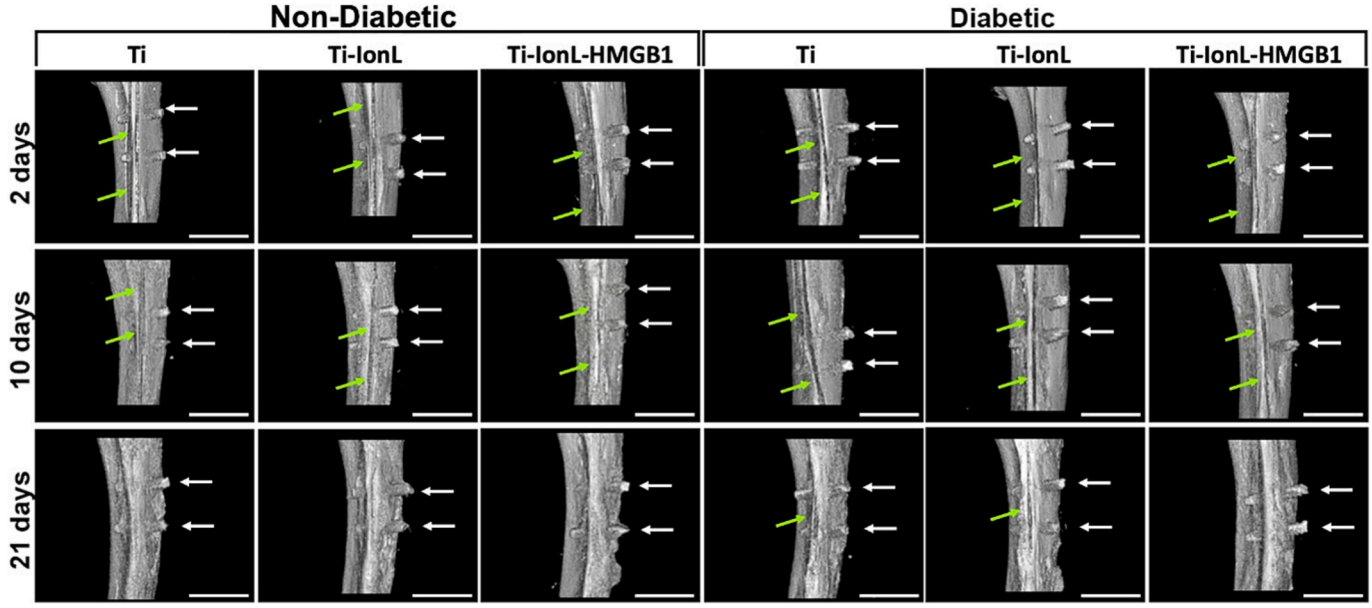

Fig. 4. Coronal microCT images of tibial implantation sites in normoglycemic and diabetic Lewis rats at 2, 10 and 21 days for uncoated Ti control (Ti), IonL-coated Ti (Ti-IonL), and HMGB1-coated Ti implants (Ti-Ion-HMGB1) ($n = 6$ independent, qualitative analyses per systemic condition, time point, and treatment). Green diagonal arrows indicate the presence of fracture gap, white horizontal arrows indicate the location of Ti implants (Scale bar = 3.5 mm). (For interpretation of the references to colour in this figure legend, the reader is referred to the web version of this article.)

cells with fibroblast morphology was found in D rats treated with Ti and Ti-IonL. Alternatively, D animals treated with Ti-IonL-HMGB1 presented improved bone formation in the fracture gap at 10 days as compared to the other D treatment groups, and a similar pattern was observed in ND animals at the same time point. Interestingly, new bone formation was identified in the screw area of all treatment groups for D animals at the 10-day time point. At the 21-daytime point, D rats treated with uncoated Ti screws presented a predominance of fibrous connective tissue and minimal bone deposition in the fracture area; however, this same treatment group resulted in osseointegrated screw threads. The Ti-IonL treated D rats presented a closure in the fracture gap, with substantial amounts of bone marrow, indicating mature bone. D rats treated with Ti-IonL-HMGB1 presented a substantial amount of bone matrix formation, surrounded by bone marrow, with no morphological differences as compared to ND rats for all treatment groups.

Bone to implant contact (BIC %) was quantified at 21 days post-implantation using (GT) with Alcian Blue-stained samples (Fig. 7A). Overall, the ND group resulted in higher bone formation surrounding the implant area in the uncoated Ti (74.70 ± 2.33 %) and Ti-IonL treated samples (72.10 ± 4.94 %) compared to the D group (61.75 ± 3.31 % for uncoated Ti and 56.82 ± 9.63 % for Ti-IonL, respectively). However, Ti-IonL-HMGB1 samples had no statistical difference in BIC % between the D group (71.36 ± 3.22 %) and the ND group (69.50 ± 7.70 %), which were also not very different from the ND Ti samples. The Ti ND group resulted in significantly higher ($p < 0.004$) bone formation surrounding the implant compared to the Ti-IonL D group. The Ti-IonL D group was also significantly different from the Ti-IonL ND ($p < 0.03$) and Ti-IonL-HMGB1 D ($p < 0.03$) samples.

Fracture healing was quantified at 2-, 10- and 21-days post-implantation by increased bone hyperdensity in terms of bone volume to tissue volume (BV/TV %) (Table S4). Fracture closure was determined as the ratio of increase between the 2- and 21-day time points (Fig. 7B and Table S5). ND animals resulted in significantly higher ($p \leq 0.05$) mineralized bone deposition in the fracture gap for uncoated Ti (14.35 ± 4.42 %) compared to D animals (9.49 ± 3.23 %) as shown in Fig. 7B. Conversely, D animals treated with Ti-IonL-HMGB1 developed significantly higher fracture closure (18.73 ± 5.06 %) compared to the D Ti-IonL (5.69 ± 2.44 %, $p \leq 0.05$) or the D uncoated Ti group (9.49 ± 3.23 %, $p \leq 0.05$) (Table S5). Trabecular bone thickness was also evaluated at the fracture site (Fig. S1). All groups, regardless of systemic condition or implant treatment resulted in similar bone trabecular thickness ($p > 0.05$).

3.5. Healing markers on osseointegration and fracture sites

Healing markers were evaluated for cell proliferation (PCNA+ cells), osteoblast differentiation (RUNX2+ cells), and the presence of HMGB1 positive cells or positive staining in sites of fracture healing (Fig. 8) and osseointegration (Fig. 9). Positively stained cells were quantified and compared in Fig. 10 and Table S6. Both ND and D animals had higher PCNA+ cells in the fracture area at 10 days compared to 2 and 21 days in Ti and Ti-IonL samples. Yet, PCNA+ cells in the tissues surrounding the implant area had a decreasing trend between 2 and 21 days for all treatment groups and systemic conditions, but resulted in a significant peak in D samples treated with Ti-IonL and Ti-IonL-HMGB1 implants at 21 days. PCNA+ cells in the tissues surrounding the implant area were also higher at all time points for Ti ND compared to Ti D. However, cell proliferation was significantly highest ($p \leq 0.0001$) in Ti-IonL-HMGB1 D samples in both the fracture and implant area.

The highest values for RUNX + cells were quantified in all animals at 10 days, with statistical differences comparing ND animals with Ti and Ti-IonL to D animals in the corresponding treatments groups. Alternatively, the Ti-IonL-HMGB1 D resulted in more populous RUNX2+ cells compared to Ti-IonL-HMGB1 ND at 10 days. At 21 days, a significantly high area density percent of RUNX2+ cells in both the fracture and implant areas are present for groups treated with Ti-IonL-HMGB1 compared to Ti or Ti-IonL, regardless of systemic condition. Congruent trends were observed in RUNX2+ cells between the fracture and implant areas.

For immunohistochemical analysis of the HMGB1 present in the cell nuclei and cytoplasm (the cellular compartments for endogenous HMGB1) of the fracture area, all 2-day samples were very similar, with a significant rise at 10 days for all samples (except Ti-IonL-HMGB1 D that was significantly lower ($p \leq 0.0001$)). At 21 days, the fracture area samples resulted in higher HMGB1+ cells for all D samples compared to ND samples. A similar trend was depicted by the area density % of

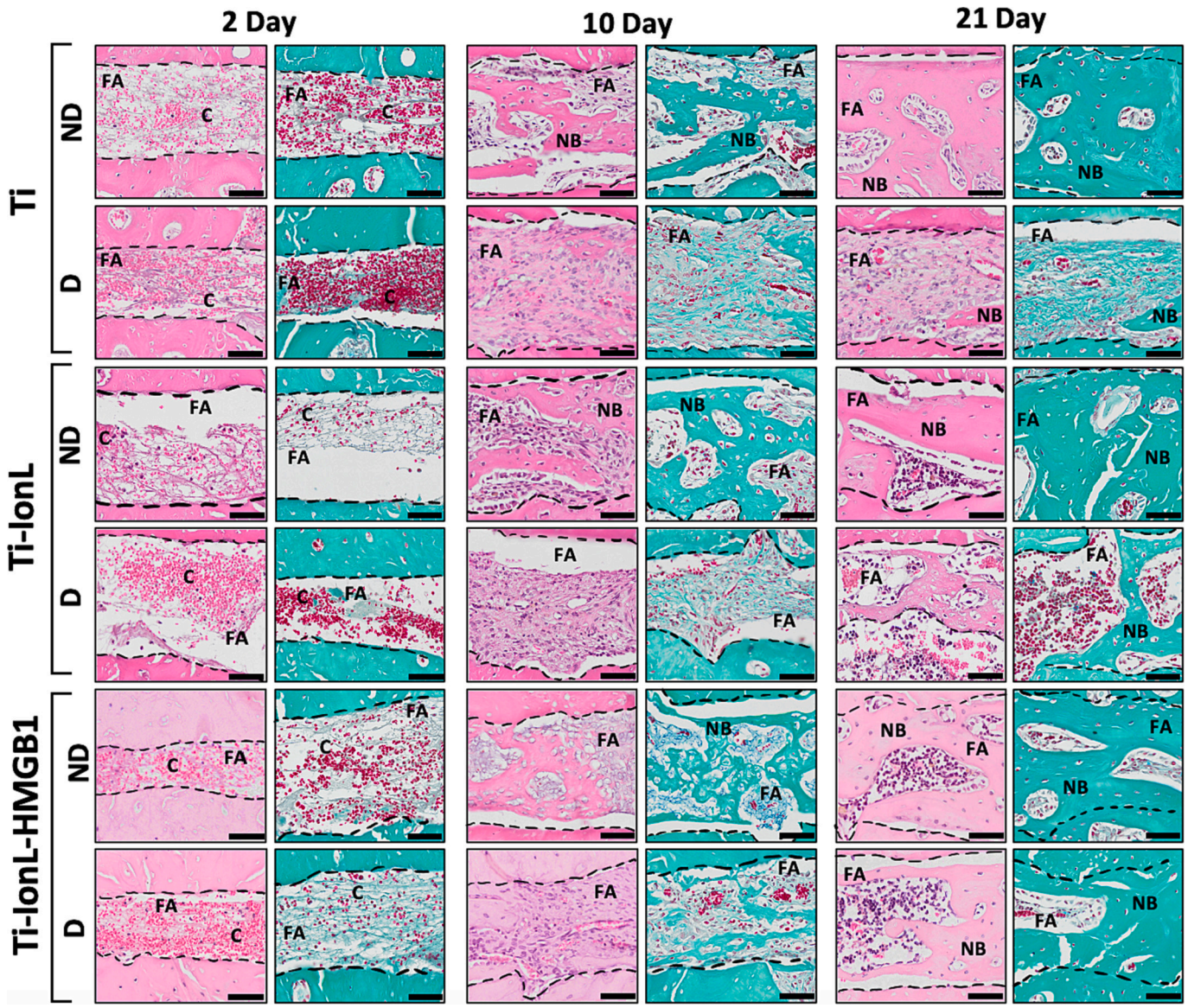

Fig. 5. Histological evaluation of fracture sites in non-diabetic (ND) and diabetic (D) rats treated with uncoated (Ti), ionic liquid coated (Ti-IonL) and HMGB1 (Ti-IonL-HMGB1) coated implants at 2, 10 and 21 days after ORIF procedure ($n = 6$ per systemic condition, time point, and treatment). Fracture area (FA) and blood clots (C) and new bone (NB) are demonstrated between dashed lines. Scale bar = 20 μm, staining: H&E (pink/purple) and GT (magenta/turquoise), original magnification 40×. (For interpretation of the references to colour in this figure legend, the reader is referred to the web version of this article.)

HMGB1+ cells in the screw area of all samples at 21 days. However, different trends were evidenced for the implant area at 2 and 10 days compared to the fracture area. Specifically, higher area density % of HMGB1 + cells resulted in Ti-IonL-HMGB1 treated cells compared to tissues surrounding Ti and Ti-IonL samples, regardless of systemic condition. At 10 and 21 days, the highest area density % of HMGB1 in the implant area was detected in the D group compared to ND within each treatment group. Also noted at 10 and 21 days, the Ti-IonL D samples were highest in the screw area compared to Ti D or Ti-IonL-HMGB1 D samples. Values for cell proliferation, osteoblast differentiation and HMGB1 receptors in tissues surrounding the fracture and screw area over time are graphically demonstrated in Fig. 10 and quantified in Table S6.

4. Discussion

Studies have shown that physical (topography, hydrophilicity) and chemical (ceramic, synthetic or peptide coatings) modifications to Ti surfaces have been employed to modulate tissue responses [36,37]. In the present study, we used IonL to anchor the immunomodulatory HMGB1 protein onto the Ti surface in a biologically active conformation. However, before performing the ORIF procedure and inducing diabetes, it was important to verify that the coating would remain on the screws pre- and post-implantation to ensure the direct and local delivery of HMGB1 to the site of trauma. IonL-based coatings had previously been shown to be stable on Ti surfaces pre- and post-implantation in the edentulous alveolar crest of Lewis rats [45]. Yet, these studies did not demonstrate the stability of the coating with HMGB1 after insertion. In the present study, uncoated Ti screws had a rough surface, while Ti-IonL screws exhibited droplet-like coalescence in the ridges of the screw, which was consistent with previous literature [45]. After removal, Ti-IonL screws continued to have IonL present, yet resulted in less visually adherent biological debris compared to uncoated Ti screws, exhibiting lubricative behavior that has been characterized in prior research [30]. The Ti-IonL-HMGB1 screws formed a crystal-like structure, which was consistent with previous observations on discs [33]. Previous

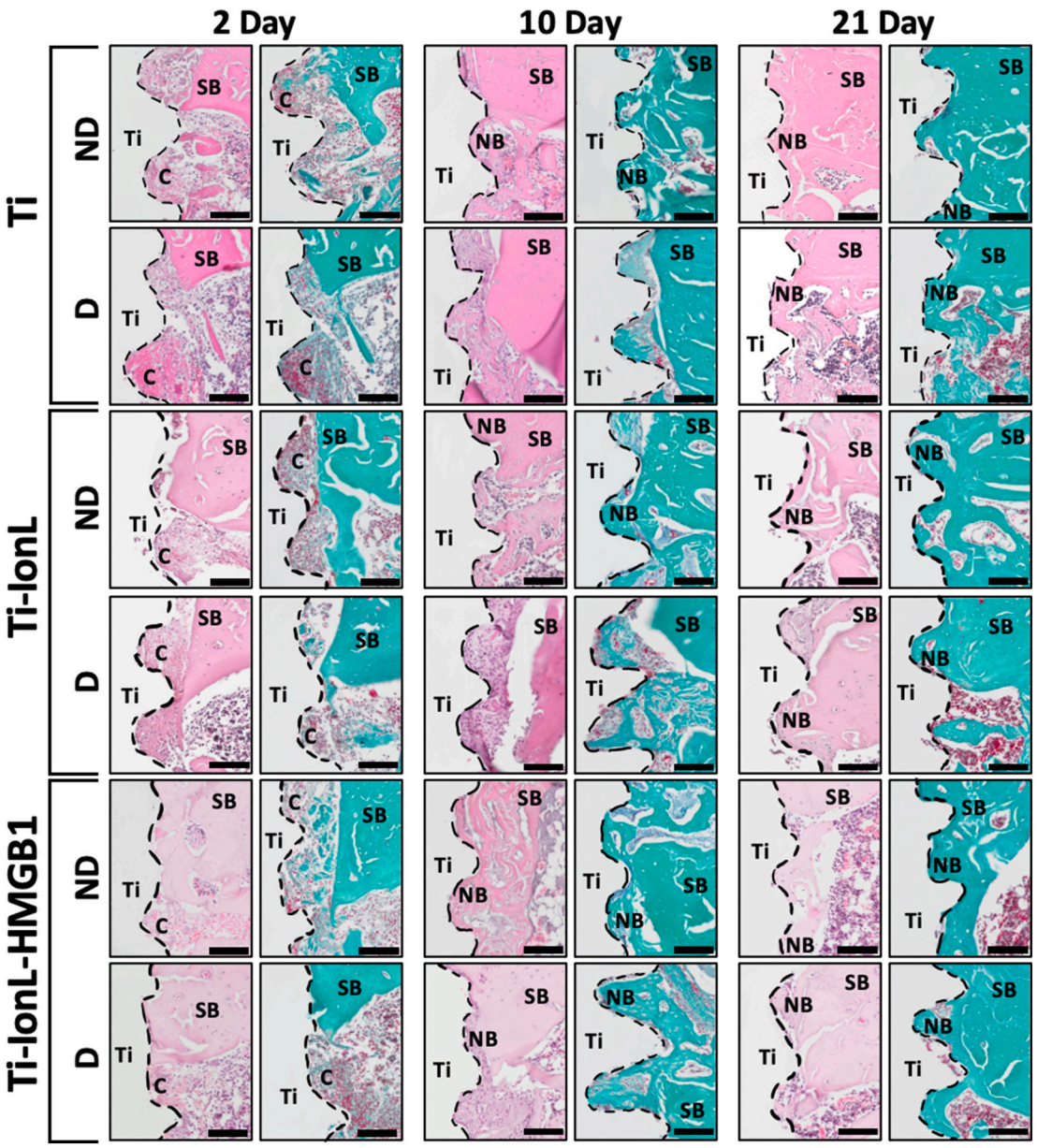

Fig. 6. Histological evaluation of implantation sites in ND and D rats treated with uncoated (Ti), ionic liquid coated (Ti-IonL) and HMGB1 coated (Ti-IonL-HMGB1) implants at 2, 10 and 21 days after implant placement (n = 6 per systemic condition, time point, and treatment). Ti implant space (Ti) is demonstrated in the white region between dashed lines, surrounding histological structures include supporting bone (SB), new bone (NB) and blood clot (C). Scale bar = 20 μm, staining: H&E (top) and GT (bottom), original magnification 40×.

studies demonstrated that the long alkyl chain lengths of ionic liquids allowed for membrane proteins to crystallize, which promoted stability onto the ionic liquids and allowed the proteins to remain biologically active [58,59]. The crystal-like structure remained present post-implantation, which demonstrated that the exogenous HMGB1 was successfully delivered at the implant sites and remained intact.

The diabetes induction throughout this study was validated through clinical characteristics such as increased water consumption for D rats after STZ administration, which is consistent with previous literature [54]. Rats fed with a HFD and received an STZ injection resulted in significantly higher levels of fasting blood glucose, during the insulin resistance test, compared to rats that were only fed a HFD or normal food, which correlates to other studies that specifically fed rats with HFD and STZ injections [60]. ND rats continued to have normal and large pancreatic islets were present, while atrophy and vacuolation were noted along with the disruption of pancreatic beta islet cells in D rats, which has also been previously demonstrated [61]. MicroCT analysis of control legs qualitatively demonstrated reduced cortical region areas in D animals compared to ND animals, indicative of reduced bone quality in D animals [6,17,62]. Mean glucose values for ND rats were consistently <250 mg/dL and significantly lower than the average values for D rats, which were consistently >250 mg/dL. These results were consistent with results published in a previous study [54]. Hyperglycemia in a rat model has been associated with elevated serum HMGB1 levels, which can contribute to chronic low-grade inflammation, which is associated with insulin resistance [63]. Considering that HMGB1 is involved in the body's stress response, the release of cortisol and catecholamines can further raise blood glucose levels by promoting the breakdown of glycogen in the liver and reducing glucose uptake by peripheral tissues [64]. Although a clinical characteristic of diabetes is weight loss, animals presented minimal weight loss as compared to ND animals, which likely was a result of the time frame that they were allowed to remain

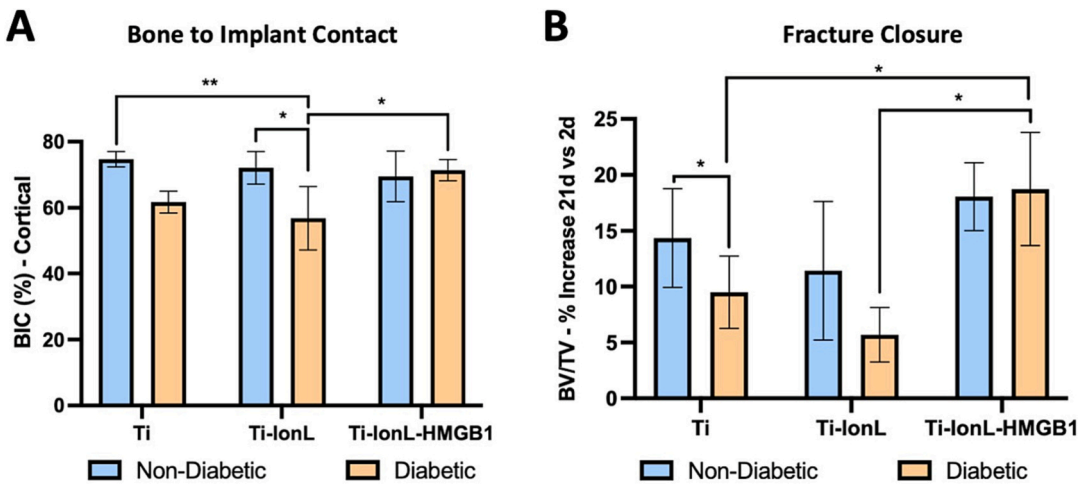

Fig. 7. BIC quantification *(A)* and fracture closure *(B)* at 21 days are shown as means ± SD (*: $p \leq 0.05$ and **: $p \leq 0.01$) between implant treatments (uncoated (Ti), ionic liquid coated (IonL: Ti-IonL) and IonL-HMGB1 coated Ti (HMGB1: Ti-IonL-HMGB1)) and/or systemic conditions (diabetic vs. non-diabetic) ($n = 5$).

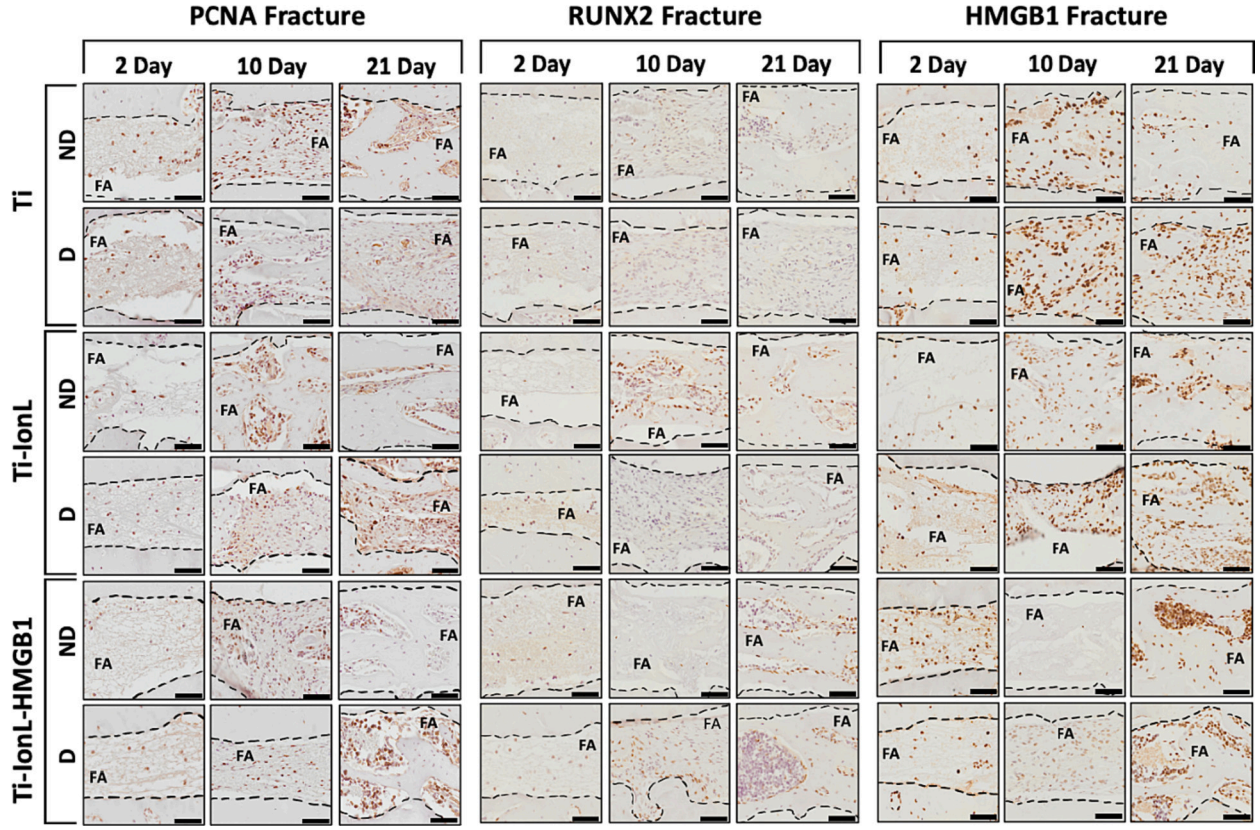

Fig. 8. Immunohistochemistry for PCNA (left), RUNX2 (middle), and HMGB1 (right) markers at the fracture sites for non-diabetic (ND) and diabetic (D) rats treated with uncoated (Ti), ionic liquid coated (Ti-IonL) and IonL-HMGB1 coated Ti (Ti-IonL-HMGB1) implants at 2, 10, and 21 days ($n = 6$ per systemic condition, time point, and treatment). Dark brown cells: positive labeling. Scale bar: 20 μm, original magnification 40×, counterstaining Mayers hematoxylin, chromogen DAB. (For interpretation of the references to colour in this figure legend, the reader is referred to the web version of this article.)

diabetic. Following this validation, we also observed that the ORIF procedure had a 100 % survival rate, no animals were lost due to surgery or implant treatment.

Local fracture healing and osseointegration in ND and D rats following the different treatments was evaluated. The ND group demonstrated signs of fracture closure, while the D group still had the fracture present at 21 days for animals treated with uncoated Ti and Ti-IonL implants. Individuals with uncontrolled glycemic levels have been shown to have relatively higher bone mineral density with lower bone quality, which normally results in increased fracture risks in patients with type 2 diabetes [17,18]. Although animals remained in an uncontrolled (no insulin administration) diabetic state, D animals treated with Ti-IonL-HMB1implants demonstrated signs of improved osseous healing in the fracture area. These results correlate with previous studies that have shown that the local administration of HMGB1 promotes bone generation in in critical fractures [65], and also imply that the IonL thin film did not interfere with the biological function of HMGB1.

In our histological evaluations, the progression of fracture healing

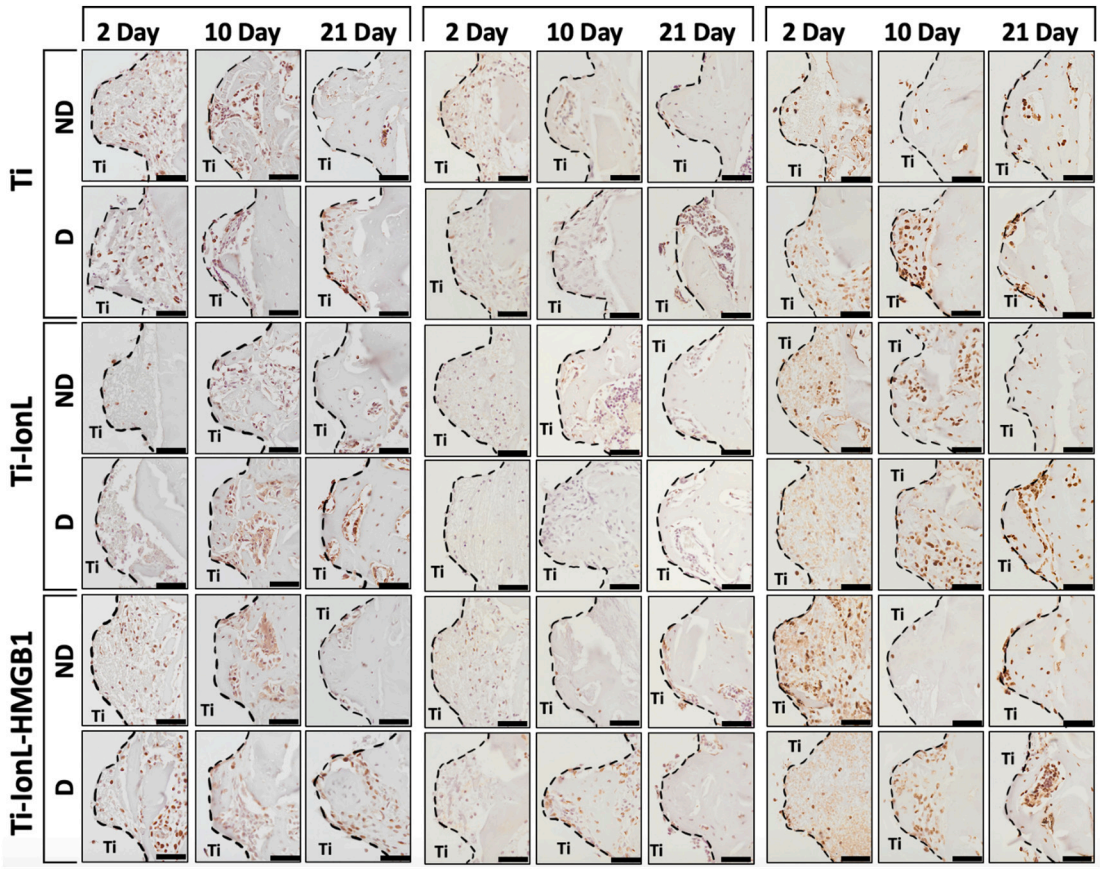

Fig. 9. Immunohistochemistry for PCNA (left), Runx2 (middle), and HMGB1 (right) markers at the implantation sites for non-diabetic (ND) and diabetic (D) rats treated with uncoated (Ti), ionic liquid coated (Ti-IonL) and IonL-HMGB1 coated Ti (Ti-IonL-HMGB1) implants at 2, 10, and 21 days (n = 6 per systemic condition, time point, and treatment). Implant space (Ti) is demonstrated between dashed lines. Dark brown cells: positive labeling. Scale bar: 20 μm, original magnification 40×, counterstaining Mayers hematoxylin, chromogen DAB. (For interpretation of the references to colour in this figure legend, the reader is referred to the web version of this article.)

and osseointegration was observed at the implant site over time. Upon the surgical procedure, blood clot formation present in the fracture and screw areas (for all systemic and treatment groups) correlated with hematoma formation and early inflammatory events [66]. Preliminary signs of new bone formation in the fracture area occurred earlier for all ND animals as compared to D animals, where a predominance of fibrous connective tissue and minimal bone deposition was noted in the fracture area, consistent with consistent with bone healing dynamics between non-diabetics and delayed osseous healing in diabetics [62]. Histological evaluations revealed trabeculae permeating the implant thread spaces of ND rats for all treatment groups, which corresponded to normal bone healing for normoglycemic animals [67,68]. Considering that D rats demonstrated earlier formation of new bone and increased fracture closure fold change in animals treated with Ti-IonL-HMGB1 compared to uncoated Ti and Ti-IonL indicates that the local administration of HMGB1 could be beneficial to bone healing as has previously been demonstrated in prior studies [65].

Altogether, fracture and osseointegration results confirmed delayed healing in D animals compared to ND animals, which is in agreement with the literature [69,70]. Osseointegration normally leads to the formation of supporting bone and preosteoblastic cells at the Ti/tissue interface [71]. Histological samples of the cortical supporting bone regions surrounding the implant space were further evaluated by bone to implant contact percent (BIC %) for quantification and comparison. It was noted that ND animals consistently resulted in higher BIC% for Ti and Ti-IonL treatment groups when compared to D animals. Interestingly, D animals treated with Ti-IonL-HMGB1 developed a similar BIC% compared to ND animals from all treatment groups. Considering the new bone formation in the ND group treated with uncoated Ti, previous studies have reported that hypertrophic chondrocytes, which can become osteoblasts and osteocytes in endochondral bone formation [72], are shown to be present at 2 weeks [73], with cancellous bone formation at 3 weeks.

Fracture healing and osseointegration were further assessed through immunohistochemical quantification for bone (RUNX2), proliferation (PCNA), and HMGB1 markers. Positively stained PCNA cells in the fracture area significantly increased from 2 to 10 days for all treatment groups, which implied initial stabilization of bone matrix onto the implant surface. However, PCNA+ cells subsided at 21 days for all groups except for D animals with Ti-IonL-HMGB1 implants, potentially indicating less proliferating cells and impaired bone tissue regeneration [74]. The quantity of PCNA+ cells surrounding the implant area remained constant for all treatment groups and time points, yet became most populous for D animals treated with Ti-IonL and Ti-IonL-HMGB1 at 21 days, demonstrating delayed osseointegration. Iwaki et al. previously described the increased amount of PCNA+ cells on the 10th day of fracture repair as premature osteoblasts and endothelial cells [75]. RUNX2 plays a dominant role in chondrocyte maturation, which induces cartilage formation, endochondral ossification and osteoblast differentiation [76]. The increased trend of RUNX2+ cells in the fracture and implant areas of both D and ND animals treated with uncoated Ti at 10 days followed by a decreased amount at 21 days are indicative of endochondral ossification events [77]. ND groups treated with Ti-IonL and also the D group treated with Ti-IonL-HMGB1 resulted in similar trends in both the fracture and screw area. Considering that the D group treated with Ti-IonL-HMGB1demonstrated hyperdense bone formation

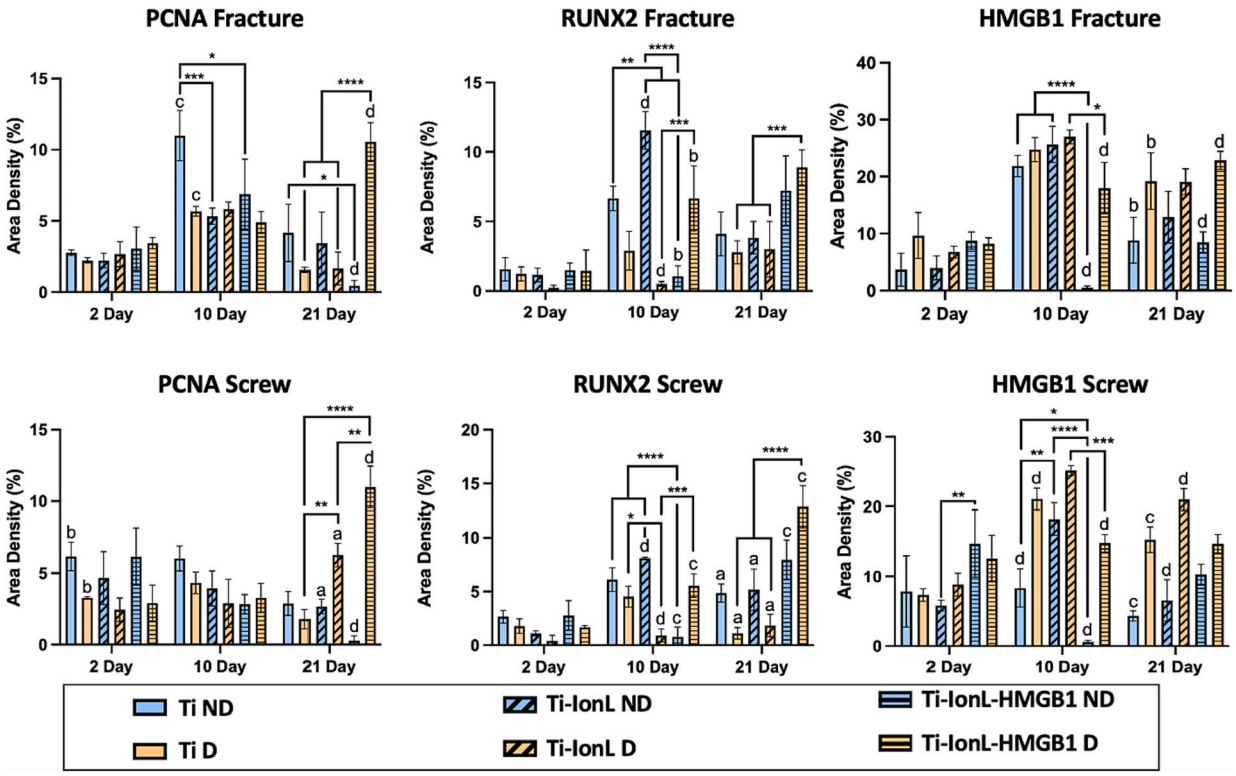

Fig. 10. Graphical quantification of PCNA, RUNX2 and HMGB1 markers identified by immunohistochemical analysis in D and ND rats and are shown as means ± SD for area density (%) at the fracture and implant sites of screws (* = $p \leq 0.05$, ** = $p \leq 0.01$, *** = $p \leq 0.001$) between treatments (uncoated (Ti), ionic liquid coated (Ti-IonL) and IonL-HMGB1 coated Ti (Ti-IonL-HMGB1)) and systemic conditions (D vs. ND; a: $p \leq 0.05$, b: $p \leq 0.01$, c: $p \leq 0.001$ and d: $p \leq 0.0001$) within the same treatments. Quantitative results are presented as mean ± SD for each parameter at the fracture area (top) and implant sites of screws (bottom) for each time point at 2, 10 and 21 days ($n = 5$).

at 21 days there was likely increased cell proliferation or osteoblast differentiation in response to the coating.

In this study, an exogenous, non-oxidizable fully reduced isoform was used that may have impacted the expression of endogenous HMGB1. From the immunohistochemical analysis, HMGB1+ staining was only observed in the cell nuclei and cytoplasm of the fracture area and the tissues surrounding implant area. Similar amounts of HMGB1+ cells were present in all treatment groups for both the fracture and the tissues surrounding the implant area at the 2-day time point for D and ND animals, which was likely a result of cellular trauma and necrotic cell death [78,79]. An increased amount of HMGB1+ cells were present in the fracture and screw area at the 10-day time point for all treatment and systemic groups, except for the ND animals treated with Ti-IonL-HMGB1. Yet, at 21 days post-implantation, the HMGB1+ cells subsided for the ND animals, while remaining consistently elevated for the D animals. Considering that HMGB1 is redox sensitive, HMGB1 that is released as a fully reduced isoform can become exposed to increased ROS that oxidize HMGB1 into a dimerized disulfide isoform, and further induces the proinflammatory response [80]. Additionally, diabetic patients experience chronic inflammation that typically plays a key role in the pathophysiology of metabolic abnormalities [81]. In this study, the HMGB1+ staining was nondiscriminatory of the isoform. Since diabetic patients normally experience chronic inflammation, elevated HMGB1+ cells at 21 days post-implantation (in both implant and fracture areas) likely correlated with chronic inflammatory events in D animals. Liu et al. demonstrated similar results, showing that HMGB1 remained elevated for the diabetic group, which was indicative of osseous fracture healing impairment and lack of Ti osteointegration in rat tibias [82].

Previous peptide coating modifications have harnessed polydopamine to immobilize a mixture of peptides (including GL13K, BFP-1, and BMP2) to promote integrin-mediated cell-matrix adhesion mechanisms that induce osteoblast differentiation *in vitro*[84,85]. However, uniform coatings of polydopamine are difficult to achieve, causing unexpected variations in performance [83]. Considering that proteins tend to denature upon adsorption on Ti surfaces, it is imperative to have a uniform coating that protects the protein in a biologically active conformation. Ultimately, to the best of our knowledge, this is the first approach to examine IonL as an anchoring coating for immunomodulatory proteins (such as 3S-HMGB1) in orthopedic applications in ND and D rats using an ORIF technique.

Although proper characterization in terms of physical, chemical and biological properties was performed, there are still several areas that can be further investigated. Although this study attempted to mimic a diabetic environment, limitations need to be discussed. Comorbidities and complications associated with diabetes are challenging to replicate. This study included only a snapshot where only male animals within a specific age range were used, so future studies should include both genders, longer time frames, genetically diabetic animal models, and controlled (application of insulin) vs. uncontrolled diabetes to gain a better understanding of comorbidities and complications in the general population. The protein layer created during early inflammatory responses should be analyzed to fully explore the overall benefits of this approach to prevent comorbidities and complications in diabetic environments. Understanding the sequelae of inflammatory responses to injury can pave the way for various immunomodulatory proteins that can be used for biomedical applications. Incorporating a push-out analysis into subsequent osseointegration studies would provide valuable quantitative data on how the coating affects interfacial strength over time. This will be conducted in a follow up study. Further exploration of functional benefits, potential side effects and the optimization of alternative proteins in combination with IonLs should be further explored for future IonL-protein based therapies.

To the best of our knowledge, this work presented for the first time dicationic imidazolium-based IonLs as a thin film to anchor immunomodulatory proteins in order to improve the surface performance of orthopedic implants. This study demonstrated the effectiveness of the Ti-IonL-HMGB1 coating using an ORIF model in diabetic and non-diabetic rats. Diabetic animals treated with Ti-IonL-HMGB1 demonstrated fracture healing and osseointegration that was comparable to non-diabetic animals. MicroCT, histological and immunohistochemical analysis of cell proliferation (PCNA), osteoblast differentiation (RUNX2), and HMGB1 markers revealed improved osseous healing in diabetic animals treated with Ti-IonL-HMGB1 coatings. The results presented in this work demonstrate that this surface approach has a great potential to improving the predictability of orthopedic implanted biomaterials in diabetic environments. Further studies are necessary for a better understanding of immunomodulatory mechanisms and multifunctionality of HMGB1-IonL based coating on diabetic healing.

CRediT authorship contribution statement

Alexandra Arteaga: Writing – review & editing, Writing – original draft, Visualization, Validation, Project administration, Methodology, Investigation, Formal analysis, Data curation, Conceptualization. **Claudia Cristina Biguetti:** Writing – review & editing, Supervision, Project administration, Methodology, Investigation, Formal analysis, Conceptualization. **BhuvanaLakkasetter Chandrashekar:** Methodology. **Javier La Fontaine:** Conceptualization. **Danieli C. Rodrigues:** Writing – review & editing, Supervision, Conceptualization.

Declaration of competing interest

None.

Data availability

Data will be made available on request.

Acknowledgements

The authors would like to acknowledge the support from the National Institute of Diabetes and Digestive and Kidney Diseases (NIDDK/NIH) F31 fellowship number F31DK121483-01. This project is also supported by the University of Texas at Dallas (UTD) Office of Research through a seed grant, Collaborative Biomedical Research Award (CoBRA), and the Eugene McDermott Graduate Fellowship (201901). The authors would like to thank Dr. Kenneth Hoyt and Ryan Margolis for the use of the Small Animal Imaging Facility at the University of Texas at Dallas. The authors would also like to thank Adeena Qureshi, Jimena Mora, and Evelin Rios for technical assistance.

Appendix A. Supplementary data

Supplementary data to this article can be found online at https://doi.org/10.1016/j.bone.2023.116917.

References

[1] D.K. Wukich, A.J. Kline, The Management of Ankle Fractures in patients with diabetes, J. Bone Joint Surg. Am. 90 (7) (2008) 1570–1578, https://doi.org/10.2106/JBJS.G.01673.
[2] T.G. Myers, N.J. Lowery, R.G. Frykberg, D.K. Wukich, Ankle and Hindfoot fusions: comparison of outcomes in patients with and without diabetes, Foot Ankle Int. 33 (1) (2012) 20–28, https://doi.org/10.3113/FAI.2012.0020.
[3] H.F. Morris, S. Ochi, S. Winkler, Implant survival in patients with type 2 diabetes: placement to 36 months, Ann. Periodontol. 5 (1) (2000) 157–165, https://doi.org/10.1902/annals.2000.5.1.157.
[4] G.K. Kolluru, S.C. Bir, C.G. Kevil, Endothelial dysfunction and diabetes: effects on angiogenesis, vascular remodeling, and wound healing, Int J Vasc Med 2012 (2012) 918267, https://doi.org/10.1155/2012/918267.
[5] H.F. Morris, S. Ochi, S. Winkler, Implant survival in patients with type 2 diabetes: placement to 36 months, Ann. Periodontol. 5 (1) (2000) 157–165, https://doi.org/10.1902/annals.2000.5.1.157.
[6] L.J. Melton, C.L. Leibson, S.J. Achenbach, T.M. Therneau, S. Khosla, Fracture risk in type 2 diabetes: update of a population-based study, J. Bone Miner. Res. 23 (8) (2008) 1334–1342, https://doi.org/10.1359/jbmr.080323.
[7] N. Shibuya, M.L. Davis, D.C. Jupiter, Epidemiology of foot and ankle fractures in the United States: an analysis of the National Trauma Data Bank (2007 to 2011), J. Foot Ankle Surg. 53 (5) (2014) 606–608, https://doi.org/10.1053/J.JFAS.2014.03.011.
[8] R. Elsoe, S.E. Ostgaard, P. Larsen, Population-based epidemiology of 9767 ankle fractures, Foot Ankle Surg. 24 (1) (2018) 34–39, https://doi.org/10.1016/J.FAS.2016.11.002.
[9] K.B. Jones, K.A. Maiers-Yelden, J.L. Marsh, M.B. Zimmerman, M. Estin, C. L. Saltzman, Ankle fractures in patients with diabetes mellitus, J. Bone Joint Surg. (Br.) 87 (4) (2005) 489–495, https://doi.org/10.1302/0301-620X.87B4.15724.
[10] T. Schmidt, N.M. Simske, M.A. Audet, A. Benedick, C.Y. Kim, H.A. Vallier, Effects of diabetes mellitus on functional outcomes and complications after torsional ankle fracture, J. Am. Acad. Orthop. Surg. 28 (16) (2020) 661–670, https://doi.org/10.5435/JAAOS-D-19-00545.
[11] D.K. Regan, A. Manoli, L. Hutzler, S.R. Konda, K.A. Egol, Impact of diabetes mellitus on surgical quality measures after ankle fracture surgery: implications for "value-based" compensation and "pay for performance", J. Orthop. Trauma 29 (12) (2015) e483–e486, https://doi.org/10.1097/BOT.0000000000000394.
[12] J.M. Manway, C.D. Blazek, P.R. Burns, Special considerations in the Management of Diabetic Ankle Fractures, Curr. Rev. Musculoskelet. Med. 11 (3) (2018) 445–455, https://doi.org/10.1007/s12178-018-9508-x.
[13] B.R. Chrcanovic, T. Albrektsson, A. Wennerberg, Diabetes and Oral implant failure: a systematic review, J. Dent. Res. 93 (9) (2014) 859–867, https://doi.org/10.1177/0022034514538820.
[14] L. Xiao, Y.-J. Zhou, Y.-B. Jiang, M.S. Tam, L.H. Cheang, H.-J. Wang, Z.-G. Zha, X.-F. Zheng, Effect of diabetes mellitus on implant Osseointegration of titanium screws: an animal experimental study, Orthop. Surg. 14 (6) (2022) 1217–1228, https://doi.org/10.1111/os.13274.
[15] S. King, I. Klineberg, I. Levinger, T.C. Brennan-Speranza, The effect of Hyperglycaemia on Osseointegration: a review of animal models of diabetes mellitus and titanium implant placement, Arch. Osteoporos. 11 (1) (2016) 29, https://doi.org/10.1007/s11657-016-0284-1.
[16] A. Arteaga, J. Qu, S. Haynes, B.G. Webb, J. LaFontaine, D.C. Rodrigues, Diabetes as a risk factor for orthopedic implant surface performance: a retrieval and in vitro study, J Bio Tribocorros 7 (2) (2021) 51, https://doi.org/10.1007/s40735-021-00486-8.
[17] P. Samakkarnthai, J.G. Sfeir, E.J. Atkinson, S.J. Achenbach, P.W. Wennberg, P. J. Dyck, A.J. Tweed, T.L. Volkman, S. Amin, J.N. Farr, A. Vella, M.T. Drake, S. Khosla, Determinants of bone material strength and cortical porosity in patients with type 2 diabetes mellitus, J. Clin. Endocrinol. Metab. 105 (10) (2020) 3718–3729, https://doi.org/10.1210/clinem/dgaa388.
[18] J. Vavanikunnel, S. Charlier, C. Becker, C. Schneider, S.S. Jick, C.R. Meier, C. Meier, Association between glycemic control and risk of fracture in diabetic patients: a nested case-control study, J. Clin. Endocrinol. Metab. 104 (5) (2019) 1645–1654, https://doi.org/10.1210/jc.2018-01879.
[19] B. Zinman, S.M. Haffner, W.H. Herman, R.R. Holman, J.M. Lachin, B.G. Kravitz, G. Paul, N.P. Jones, R.P. Aftring, G. Viberti, S.E. Kahn, S. Kahn, Effect of rosiglitazone, metformin, and glyburide on bone biomarkers in patients with type 2 diabetes, J. Clin. Endocrinol. Metab. 95 (1) (2010) 134–142, https://doi.org/10.1210/JC.2009-0572.
[20] D.K. Wukich, Diabetes and its negative impact on outcomes in Orthopaedic surgery, World J. Orthop. 6 (3) (2015) 331, https://doi.org/10.5312/WJO.V6.I3.331.
[21] J.S. Roh, D.H. Sohn, Damage-associated molecular patterns in inflammatory diseases, Immune Netw 18 (4) (2018), e27, https://doi.org/10.4110/in.2018.18.e27.
[22] C.C. Biguetti, F. Cavalla, E.V. Silveira, A.P. Tabanez, C.F. Francisconi, R. Taga, A. P. Campanelli, A.P.F. Trombone, D.C. Rodrigues, G.P. Garlet, HGMB1 and RAGE as essential components of Ti Osseointegration process in mice, Front. Immunol. 10 (April) (2019) 709, https://doi.org/10.3389/fimmu.2019.00709.
[23] G. Lee, A.I. Espirito Santo, S. Zwingenberger, L. Cai, T. Vogl, M. Feldmann, N. J. Horwood, J.K. Chan, J. Nanchahal, Fully reduced HMGB1 accelerates the regeneration of multiple tissues by transitioning stem cells to GAlert, Proc. Natl. Acad. Sci. U. S. A. 115 (19) (2018) E4463–E4472, https://doi.org/10.1073/pnas.1802893115.
[24] Y. Yu, D. Tang, R. Kang, Oxidative stress-mediated HMGB1 biology, Front. Physiol. 6 (2015) 93, https://doi.org/10.3389/fphys.2015.00093.
[25] A.A. Alfadda, R.M. Sallam, Reactive oxygen species in health and disease, J. Biomed. Biotechnol. 2012 (2012) 1–14, https://doi.org/10.1155/2012/936486.
[26] F. Biscetti, M.M. Rando, E. Nardella, A.L. Cecchini, G. Pecorini, R. Landolfi, A. Flex, High mobility group box-1 and diabetes mellitus complications: state of the art and future perspectives, Int. J. Mol. Sci. MDPI AG December (2019), https://doi.org/10.3390/ijms20246258.
[27] E. Venereau, M. Casalgrandi, M. Schiraldi, D.J. Antoine, A. Cattaneo, F. De Marchis, J. Liu, A. Antonelli, A. Preti, L. Raeli, S.S. Shams, H. Yang, L. Varani, U. Andersson, K.J. Tracey, A. Bachi, M. Uguccioni, M.E. Bianchi, Mutually exclusive redox forms of HMGB1 promote cell recruitment or Proinflammatory cytokine release, J. Exp. Med. 209 (9) (2012) 1519–1528, https://doi.org/10.1084/jem.20120189.

[28] D. Ranathunga, A. Arteaga, C.C. Biguetti, D.C. Rodrigues, S.O. Nielsen, Molecular-level understanding of the influence of ions and water on HMGB1 adsorption induced by surface hydroxylation of titanium implants, Langmuir 37 (2021) 10100–10114, https://doi.org/10.1021/acs.langmuir.1c01444.

[29] I.M. Gindri, D.A. Siddiqui, P. Bhardwaj, L.C. Rodriguez, K.L. Palmer, C.P. Frizzo, M. A.P. Martins, D.C. Rodrigues, Dicationic imidazolium-based ionic liquids: a new strategy for non-toxic and antimicrobial materials, RSC Adv. 4 (107) (2014) 62594–62602, https://doi.org/10.1039/C4RA09906K.

[30] P.P.K. Sandhu, I.M. Gindri, D.A. Siddiqui, D.C. Rodrigues, Functional Biomaterials Dicationic Imidazolium-Based Ionic Liquid Coatings on Zirconia Surfaces: Physico-Chemical and Biological Characterization, 2017, https://doi.org/10.3390/jfb8040050.

[31] I.M. Gindri, D.A. Siddiqui, C.P. Frizzo, M.A.P. Martins, D.C. Rodrigues, Improvement of Tribological and anti-corrosive performance of titanium surfaces coated with Dicationic imidazolium-based ionic liquids, RSC Adv. 6 (82) (2016) 78795–78802, https://doi.org/10.1039/C6RA13961B.

[32] S.E. Wheelis, C.C. Biguetti, S. Natarajan, L. Guida, B. Hedden, G.P. Garlet, D. C. Rodrigues, Investigation of the early healing response to Dicationic imidazolium-based ionic liquids: a biocompatible coating for titanium implants, ACS Biomater Sci. Eng. 6 (2) (2020) 984–994, https://doi.org/10.1021/acsbiomaterials.9b01884.

[33] A. Arteaga, Dineli T.S. Ranathunga, J. Qu, C.C. Biguetti, S.O. Nielsen, D. C. Rodrigues, Exogenous Protein Delivery of Ionic Liquid-Mediated HMGB1 Coating on Titanium Implants, 2023, https://doi.org/10.1021/acs.langmuir.2c02688.

[34] Arteaga, A.; Biguetti, C. C.; Lakkasetter Chandrashekar, B.; Mora, J.; Qureshi, A.; Rodrigues, D. C. Biological effects of new titanium surface coatings based on ionic liquid and HMGB1: a cellular and molecular characterization in Lewis rats. ACS Biomater Sci. Eng.

[35] A. Arteaga, C.C. Biguetti, B. Lakkasetter Chandrashekar, J. Mora, A. Qureshi, E. Rios, J. La Fontaine, D.C. Rodrigues, A model study to evaluate osseointegration and fracture healing following open reduction and internal fixation (ORIF) in diabetic Lewis rats, J. Foot Ankle Surg. 62 (5) (2023) 832–839, https://doi.org/10.1053/j.jfas.2023.04.011.

[36] S. Shirazi, S. Ravindran, L.F. Cooper, Topography-mediated immunomodulation in osseointegration; ally or enemy, Biomaterials 121903 (2022), https://doi.org/10.1016/J.BIOMATERIALS.2022.121903.

[37] A. Civantos, E. Martínez-Campos, V. Ramos, C. Elvira, A. Gallardo, A. Abarrategi, Titanium coatings and surface modifications: toward clinically useful bioactive implants, ACS Biomater Sci. Eng. 3 (7) (2017) 1245–1261, https://doi.org/10.1021/acsbiomaterials.6b00604.

[38] A. Bandyopadhyay, I. Mitra, S.B. Goodman, M. Kumar, S. Bose, Improving biocompatibility for next generation of metallic implants, Prog. Mater. Sci. 133 (2023) 101053, https://doi.org/10.1016/j.pmatsci.2022.101053.

[39] C.C. Biguetti, F. Cavalla, E.M. Silveira, A.C. Fonseca, A.E. Vieira, A.P. Tabanez, D. C. Rodrigues, A.P.F. Trombone, G.P. Garlet, Oral implant osseointegration model in C57Bl/6 mice: microtomographic, histological, histomorphometric and molecular characterization, J. Appl. Oral Sci. 26 (e20170601) (2018) 1–16, https://doi.org/10.1590/1678-7757-2017-0601.

[40] S.E. Wheelis, C.C. Biguetti, S. Natarajan, A. Arteaga, J. El Allami, B. Lakkasettar Chandrashekar, G.P. Garlet, D.C. Rodrigues, Cellular and molecular dynamics during early Oral Osseointegration: a comprehensive characterization in the Lewis rat, ACS Biomater Sci. Eng. (2021), https://doi.org/10.1021/acsbiomaterials.0c01420.

[41] I.M. Gindri, D.A. Siddiqui, C.P. Frizzo, M.A.P. Martins, D.C. Rodrigues, Ionic liquid coatings for titanium surfaces: effect of IL structure on coating profile, ACS Appl. Mater. Interfaces 7 (49) (2015) 27421–27431, https://doi.org/10.1021/acsami.5b09309.

[42] D.A. Siddiqui, I.M. Gindri, D.C. Rodrigues, Corrosion and Wear performance of titanium and cobalt chromium molybdenum alloys coated with Dicationic imidazolium-based ionic liquids, J Bio Tribocorros 2 (4) (2016) 27, https://doi.org/10.1007/s40735-016-0057-9.

[43] I.M. Gindri, K.L. Palmer, D.A. Siddiqui, S. Aghyarian, C.P. Frizzo, M.A.P. Martins, D.C. Rodrigues, Evaluation of mammalian and bacterial cell activity on titanium surface coated with Dicationic imidazolium-based ionic liquids †, RSC Adv. 6 (43) (2016) 36475–36483, https://doi.org/10.1039/c6ra01003b.

[44] I.M. Gindri, C.P. Frizzo, C.R. Bender, A.Z. Tier, M.A.P. Martins, M.A. Villetti, G. MacHado, L.C. Rodriguez, D.C. Rodrigues, Preparation of TiO2 nanoparticles coated with ionic liquids: a supramolecular approach, ACS Appl. Mater. Interfaces 6 (14) (2014) 11536–11543, https://doi.org/10.1021/am5022107.

[45] S.E. Wheelis, S.A. Natarajan, B. Lakkasetter Chandrashekar, A. Arteaga, G. P. Garlet, D.C. Rodrigues, Effects of dicationic imidazolium-based ionic liquids on oral osseointegration of titanium implants: an in vivo biocompatibility study in multiple rat demographics, Genes (Basel) 13 (642) (2022) 1–25.

[46] K. Fukumoto, M. Yoshizawa, H. Ohno, Room temperature ionic liquids from 20 natural amino acids, J. Am. Chem. Soc. 127 (2005) 2398–2399, https://doi.org/10.1021/ja043451i.

[47] H. Shirota, T. Mandai, H. Fukazawa, T. Kato, Comparison between dicationic and monocationic ionic liquids: liquid density, thermal properties, surface tension, and shear viscosity, J. Chem. Eng. Data 56 (2011) 48, https://doi.org/10.1021/je2000183.

[48] I. de Mello Gindri, Design of multifunctional ionic liquids for surface modification of dental implants, ProQuest Dissertations and Theses 261 (2016).

[49] Y. Wang-Fischer, T. Garyantes, Improving the reliability and utility of Streptozotocin-induced rat diabetic model, J. Diabetes Res. 2018 (2018) 8054073, https://doi.org/10.1155/2018/8054073.

[50] M.J. Reed, K. Meszaros, L.J. Entes, M.D. Claypool, J.G. Pinkett, T.M. Gadbois, G. M. Reaven, A new rat model of type 2 diabetes: the fat-fed, streptozotocin-treated rat, Metabolism 49 (11) (2000) 1390–1394, https://doi.org/10.1053/META.2000.17721.

[51] M. Zhang, X.Y. Lv, J. Li, Z.G. Xu, L. Chen, The characterization of high-fat diet and multiple low-dose Streptozotocin induced type 2 diabetes rat model, Exp. Diabetes Res. 2008 (2008) 704045, https://doi.org/10.1155/2008/704045.

[52] K. Srinivasan, B. Viswanad, L. Asrat, C.L. Kaul, P. Ramarao, Combination of high-fat diet-fed and low-dose Streptozotocin-treated rat: a model for type 2 diabetes and pharmacological screening, Pharmacol. Res. 52 (4) (2005) 313–320, https://doi.org/10.1016/j.phrs.2005.05.004.

[53] N. Vatandoust, F. Rami, A.R. Salehi, S. Khosravi, G. Dashti, G. Eslami, S. Momenzadeh, R. Salehi, Novel high-fat diet formulation and streptozotocin treatment for induction of prediabetes and type 2 diabetes in rats, Advanced Biomedical Research 7 (2018) 107–112, https://doi.org/10.4103/abr.abr_8_17.

[54] X.-X. Guo, Y. Wang, K. Wang, B.-P. Ji, F. Zhou, Stability of a type 2 diabetes rat model induced by high-fat diet feeding with low-dose streptozotocin injection, J Zhejiang Univ-Sci B (Biomed & Biotechnol) 19 (7) (2018) 559–569, https://doi.org/10.1631/jzus.B1700254.

[55] C.C. Biguetti, A.H. De Oliva, K. Healy, R.H. Mahmoud, I.D.C. Custódio, D. H. Constantino, E. Ervolino, M.A.H. Duarte, W.D. Fakhouri, M.A. Matsumoto, Medication-related osteonecrosis of the jaws after tooth extraction in senescent female mice treated with zoledronic acid: microtomographic, histological and immunohistochemical characterization, PLoS One 14 (6) (2019), e0214173, https://doi.org/10.1371/journal.pone.0214173.

[56] C.C. Biguetti, F. Cavalla, A.C. Fonseca, A.P. Tabanez, D.A. Siddiqui, S.E. Wheelis, R. Taga, W.D. Fakhouri, R.M. Silva, D.C. Rodrigues, G.P. Garlet, Effects of titanium corrosion products on in vivo biological response: a basis for the understanding of osseointegration failures mechanisms, Front Mater 8 (2021) 159, https://doi.org/10.3389/fmats.2021.651970.

[57] S.G. Sotocinal, R.E. Sorge, A. Zaloum, A.H. Tuttle, L.J. Martin, J.S. Wieskopf, J.C. S. Mapplebeck, P. Wei, S. Zhan, S. Zhang, J.J. McDougall, O.D. King, J.S. Mogil, The rat grimace scale: a partially automated method for quantifying pain in the laboratory rat via facial expressions, Mol. Pain 7 (2011) 55, https://doi.org/10.1186/1744-8069-7-55.

[58] B.D. Belviso, R. Caliandro, S.M. Salehi, G. Di Profio, R. Caliandro, Protein crystallization in ionic-liquid hydrogel composite membranes, Crystals (Basel) 9 (5) (2019) 253, https://doi.org/10.3390/cryst9050253.

[59] C. Schröder, Proteins in ionic liquids: current status of experiments and simulations, Top. Curr. Chem. 375 (2) (2017) 25, https://doi.org/10.1007/s41061-017-0110-2.

[60] P.C. Chao, Y. Li, C.H. Chang, J.P. Shieh, J.T. Cheng, K.C. Cheng, Investigation of insulin resistance in the popularly used four rat models of Type-2 diabetes, Biomed. Pharmacother. 101 (2018) 155–161, https://doi.org/10.1016/j.biopha.2018.02.084.

[61] T. Szkudelski, The mechanism of alloxan and streptozotocin action in B cells of the rat pancreas, Physiol. Res. 50 (2001) 536–546.

[62] H. Jiao, E. Xiao, D.T. Graves, Diabetes and its effect on bone and fracture healing, Curr. Osteoporos. Rep. 13 (5) (2015) 327–335, https://doi.org/10.1007/s11914-015-0286-8.

[63] S. Hagiwara, H. Iwasaka, A. Hasegawa, H. Koga, T. Noguchi, Effects of hyperglycemia and insulin therapy on high mobility group box 1 in endotoxin-induced acute lung injury in a rat model, Crit. Care Med. 36 (8) (2008) 2407–2413, https://doi.org/10.1097/CCM.0B013E318180B3BA.

[64] I. Nomikos, M. Kyriazi, D. Vamvakopoulou, A. Sidiropoulos, A. Apostolou, A. Kyritsaka, E. Athanassiou, N.C. Vamvakopoulos, On the Management of Hyperglycaemia in critically ill patients undergoing surgery, J. Clin. Med. Res. 4 (4) (2012) 237, https://doi.org/10.4021/JOCMR604W.

[65] A. Monir, T. Mukaibo, A. Basit, M. Abd El-Aal, T. Nodai, T. Munemasa, Y. Kondo, C. Masaki, M.A. El-Shair, K. Matsuo, R. Hosokawa, Local administration of HMGB-1 promotes bone regeneration on the critical-sized mandibular defects in rabbits, Sci. Rep. 11 (2021) 8950, https://doi.org/10.1038/s41598-021-88195-7.

[66] J.M. Anderson, Inflammatory response to implants, ASAIO Trans. 34 (2) (1988) 101–107.

[67] J.D. Miles, P. Weinhold, O. Brimmo, L. Dahners, Rat Tibial osteotomy model providing a range of Normal to impaired healing, J. Orthop. Res. 29 (1) (2011) 109–115, https://doi.org/10.1002/jor.21194.

[68] E. Shi, G. Chen, B. Qin, Y. Yang, J. Fang, L. Li, Y. Wang, M. Zhu, J. Yang, L. Gu, A novel rat model of tibial fracture for trauma researches: a combination of different types of fractures and soft tissue injuries, J. Orthop. Surg. Res. 14 (1) (2019) 333–343, https://doi.org/10.1186/s13018-019-1386-4.

[69] S. Patel, S. Srivastava, M.R. Singh, D. Singh, Mechanistic insight into diabetic wounds: pathogenesis, molecular targets and treatment strategies to pace wound healing, Biomed. Pharmacother. 112 (2019) 108615, https://doi.org/10.1016/J.BIOPHA.2019.108615.

[70] J.J. Salazar, W.J. Ennis, T.J. Koh, Diabetes medications: impact on inflammation and wound healing, J. Diabetes Complicat. 30 (4) (2016) 746–752, https://doi.org/10.1016/j.jdiacomp.2015.12.017.

[71] A. Schindeler, M.M. McDonald, P. Bokko, D.G. Little, Bone remodeling during fracture repair: the cellular picture, Semin. Cell Dev. Biol. 19 (5) (2008) 459–466, https://doi.org/10.1016/j.semcdb.2008.07.004.

[72] Yang, L.; Yeung Tsang, K.; Ching Tang, H.; Chan, D.; Cheah, K. S. E. Hypertrophic chondrocytes can become osteoblasts and osteocytes in endochondral bone formation. Proc. Natl. Acad. Sci. U. S. A. 111 (33), 12097–12102. doi:https://doi.org/10.1073/pnas.1302703111.

[73] K.O. Handool, S.M. Ibrahim, U. Kaka, M.A. Omar, J. Abu, M.S.M. Yusoff, L. M. Yusof, Optimization of a closed rat tibial fracture model, J Exp Orthop 5 (1) (2018) 13–22, https://doi.org/10.1186/s40634-018-0128-6.
[74] C. Wallner, J. Schira, J.M. Wagner, M. Schulte, S. Fischer, T. Hirsch, W. Richter, S. Abraham, U. Kneser, M. Lehnhardt, B. Behr, Application of VEGFA and FGF-9 enhances angiogenesis, osteogenesis and bone remodeling in type 2 diabetic long bone regeneration, PLoS One 10 (3) (2015) 118823, https://doi.org/10.1371/journal.pone.0118823.
[75] A. Iwaki, S. Jingushi, Y. Oda, T. Izumi, J.I. Shida, M. Tsuneyoshi, Y. Sugioka, Localization and quantification of proliferating cells during rat fracture repair: detection of proliferating cell nuclear antigen by immunohistochemistry, J. Bone Miner. Res. 12 (1) (1997) 96–102, https://doi.org/10.1359/JBMR.1997.12.1.96.
[76] M.E. McGee-Lawrence, L.R. Carpio, E.W. Bradley, A. Dudakovic, J.B. Lian, A.J. van Wijnen, S. Kakar, W. Hsu, J.J. Westendorf, Runx2 is required for early stages of endochondral bone formation but delays final stages of bone repair in Axin2-deficient mice, Bone 66 (2014) 277–286, https://doi.org/10.1016/J.BONE.2014.06.022.
[77] J.R. Sheen, V.V. Garla, Fracture Healing Overview, StatPearls, 2022.
[78] M. Deng, M.J. Scott, J. Fan, T.R. Billiar, Location is the key to function: HMGB1 in sepsis and trauma-induced inflammation, J. Leukoc. Biol. (2019) 161–169, https://doi.org/10.1002/JLB.3MIR1218-497R.
[79] E.D. Peltz, E.E. Moore, P.C. Eckels, S.S. Damle, Y. Tsuruta, J.L. Johnson, A. Sauaia, C.C. Silliman, A. Banerjee, E. Abraham, HMGB1 is markedly elevated within 6 hours of mechanical trauma in humans, Shock 32 (1) (2009) 17–22, https://doi.org/10.1097/shk.0b013e3181997173.
[80] M.S. Kwak, H.S. Kim, B. Lee, Y.H. Kim, M. Son, J.S. Shin, Immunological significance of HMGB1 post-translational modification and redox biology, Front. Immunol. 11 (June) (2020) 1–16, https://doi.org/10.3389/fimmu.2020.01189.
[81] S. Tsalamandris, A.S. Antonopoulos, E. Oikonomou, G.A. Papamikroulis, G. Vogiatzi, S. Papaioannou, S. Deftereos, D. Tousoulis, The role of inflammation in diabetes: current concepts and future perspectives, European Cardiology Review 14 (1) (2019) 50, https://doi.org/10.15420/ECR.2018.33.1.
[82] B. Liu, X. Gan, Y. Zhao, H. Yu, J. Gao, H. Yu, Inhibition of HMGB1 promotes osseointegration under hyperglycemic condition through improvement of BMSC dysfunction, Oxidative Med. Cell. Longev. (2019) 1–14.
[83] S. Soulmaz, K. Mehran, D. Niyousha, L. Dejian, Y. Baoqing, The effects of process parameters on polydopamine coatings employed in tissue engineering applications, Front. Bioeng. Biotechnol. 10 (2022), https://doi.org/10.3389/fbioe.2022.1005413.